© 2021. Published by The Company of Biologists Ltd | Journal of Experimental Biology (2021) 224, jeb233098. doi:10.1242/jeb.233098

RESEARCH ARTICLE

The visual ecology of Holocentridae, a nocturnal coral reef fish family with a deep-sea-like multibank retina

Fanny de Busserolles[1,*], Fabio Cortesi[1], Lily Fogg[1], Sara M. Stieb[1,2], Martin Luehrmann[1] and N. Justin Marshall[1]

ABSTRACT

The visual systems of teleost fishes usually match their habitats and lifestyles. Since coral reefs are bright and colourful environments, the visual systems of their diurnal inhabitants have been more extensively studied than those of nocturnal species. In order to fill this knowledge gap, we conducted a detailed investigation of the visual system of the nocturnal reef fish family Holocentridae. Results showed that the visual system of holocentrids is well adapted to their nocturnal lifestyle with a rod-dominated retina. Surprisingly, rods in all species were arranged into 6–17 well-defined banks, a feature most commonly found in deep-sea fishes, that may increase the light sensitivity of the eye and/or allow colour discrimination in dim light. Holocentrids also have the potential for dichromatic colour vision during the day with the presence of at least two spectrally different cone types: single cones expressing the blue-sensitive *SWS2A* gene, and double cones expressing one or two green-sensitive *RH2* genes. Some differences were observed between the two subfamilies, with Holocentrinae (squirrelfish) having a slightly more developed photopic visual system than Myripristinae (soldierfish). Moreover, retinal topography of both ganglion cells and cone photoreceptors showed specific patterns for each cell type, likely highlighting different visual demands at different times of the day, such as feeding. Overall, their well-developed scotopic visual systems and the ease of catching and maintaining holocentrids in aquaria, make them ideal models to investigate teleost dim-light vision and more particularly shed light on the function of the multibank retina and its potential for dim-light colour vision.

KEY WORDS: Colour vision, Dim-light vision, Holocentrid, Multibank retina, Teleost fish, Nocturnal coral reef fish

INTRODUCTION

Vision in teleost fishes plays a crucial role in communication, prey detection, predator avoidance, habitat choice, and navigation (Marshall and Vorobyev, 2003; Cronin et al., 2014; Marshall et al., 2019). Because teleost fishes inhabit a broad range of environments with different light conditions and structural complexity (rivers, lakes, open ocean, deep-sea, coastal, coral reefs), have different activity patterns (nocturnal, diurnal, crepuscular) and diets (herbivory, carnivory, detrivory, planktivory), and display a variety of visually guided behaviours (courtship, communication, territorial, migratory), their visual systems had to adapt to meet these different visual demands (Walls, 1942; Collin and Shand, 2003; Warrant et al., 2003; Marshall et al., 2019; Carleton and Yourick, 2020).

These adaptations can be seen at many different levels of the visual system. At the ocular level, the shape and size of the eye and/or pupillary aperture affect the amount of light reaching the retina (Douglas and Djamgoz, 1990; Cronin et al., 2014), while filters present in the cornea or lens may modify the light spectrum before it reaches the light-sensitive opsin proteins located in the photoreceptor outer segments (Thorpe et al., 1993; Siebeck et al., 2003). At the retinal level, it is the type, size, number and distribution of the different neural cells that shape the visual system (Walls, 1942). The first level of visual processing is achieved by cone and rod photoreceptors (Lamb, 2013). Rods usually contain the highly sensitive rhodopsin protein (RH1) and mediate vision in dim-light conditions. Cones contain up to four different cone opsin proteins (short-, medium- and long-wavelength sensitive, SWS1/SWS2, RH2 and LWS, respectively) and mediate vision in bright-light conditions as well as colour vision (Yokoyama, 2008). In addition, rods and cones can vary in length and width (Ali and Anctil, 1976), and in the case of the cones, can be further divided into different morphological subtypes: single, double (two single cones fused together), triple or quadruple cones, although the last two types are relatively rare (Engström, 1963). The last level of retinal processing is performed by the ganglion cells, and their receptive field ultimately sets the upper limit of visual acuity as well as the optical sensitivity of the eye (Warrant and Locket, 2004). At the molecular level, it is the specific opsin gene repertoire, type of chromophore, as well as the level of expression of each opsin gene including the co-expression of multiple opsins within the same photoreceptor, that determines the spectral sensitivity of the photoreceptors and their capacity for colour vision (Hunt et al., 2014). All of these visual characteristics may differ between teleost species or even within the eye itself (intraocular and intraretinal variability) depending on the visual ecology, environment, and phylogenetic inertia of each species (Collin and Pettigrew, 1989; Cronin et al., 2014; Dalton et al., 2017; de Busserolles and Marshall, 2017; Stieb et al., 2019; Carleton et al., 2020).

Coral reefs are some of the most vibrant and colourful environments on the planet (McFarland, 1991). Consequently, coral reef inhabitants often have complex visual systems with well-developed colour vision capabilities. Colour vision in coral reef teleosts relies on the comparison of two to four spectrally different cone photoreceptors (di- to tetrachromatic), which may vary greatly in their spectral placement (Lythgoe, 1979; Marshall et al., 2019). This variability in spectral sensitivities seems to correlate, at least to a certain extent, with changes in the light environment due to season, habitat depth or ontogeny, and also due to differences in ecology and behaviour (Lythgoe, 1979; Shand, 1994b; Cortesi et al., 2016; Stieb et al., 2016, 2017; Tettamanti

[1]Queensland Brain Institute, The University of Queensland, Brisbane, QLD 4072, Australia. [2]Center for Ecology, Evolution and Biogeochemistry, Eawag Federal Institute of Aquatic Science and Technology, Seestrasse 79, 6074 Kastanienbaum, Switzerland; and Institute for Ecology and Evolution, University of Bern, Baltzerstrasse 6, 3012 Bern, Switzerland.

*Author for correspondence (f.debusserolles@uq.edu.au)

F.d.B., 0000-0002-4602-9840; F.C., 0000-0002-7518-6159; S.M.S., 0000-0001-7158-3934

Received 23 July 2020; Accepted 16 November 2020

Journal of Experimental Biology (2021) 224, jeb233098. doi:10.1242/jeb.233098

et al., 2019). Intraretinal variability in the distribution and density of photoreceptors and ganglion cells (i.e. retinal topography), has also been shown to vary with habitat structure (Collin and Pettigrew, 1988a,b), behavioural ecology (Stieb et al., 2019; Luehrmann et al., 2020) and ontogeny (Tettamanti et al., 2019) of coral reef fishes.

While vision in diurnal reef fishes has received substantial attention, the visual systems of nocturnal reef fishes remain understudied. From the few studies available, nocturnal reef fishes seem to have developed similar adaptations to other teleosts living in low-light environments (turbid/murky waters or the deep sea) in order to enhance the sensitivity of their eyes. These include: large eyes and pupillary apertures (Pankhurst, 1989; Schmitz and Wainwright, 2011), a smaller focal length (McFarland, 1991; Shand, 1994b), a tapetum lucidum (Nicol et al., 1973), a rod-dominated retina (Munz and McFarland, 1973; Luehrmann et al., 2020), longer and denser rods (Pankhurst, 1989; McFarland, 1991; Shand, 1994a), and an increase in the summation ratio of rods onto bipolar and ganglion cells (Shand, 1997). However, these observations are limited to few species and the opsin expression, retinal topography and most of the visual capabilities and visual ecology of nocturnal reef fishes remain understudied. A notable exception are members of the Apogonidae, which have recently been investigated in greater detail (Shand, 1997; Fishelson et al., 2004; Luehrmann et al., 2019, 2020).

To learn more about the visual world of nocturnal reef fishes, we focused our study on the Holocentridae, which comprises 91 recognised species divided into two subfamilies, the squirrelfish (Holocentrinae) and the soldierfish (Myripristinae) (Fricke et al., 2020). Holocentrids are found circumtropically and usually inhabit shallow coral reefs, although a few species, especially from the genus *Ostichthys*, occur in the deep-sea at depths of up to 640 m (Greenfield, 2002; Greenfield et al., 2017). While holocentrids are mainly active at night when they engage in feeding, they are also observed during the day hovering in or close to their refuges. Their large eyes (Schmitz and Wainwright, 2011) and ability to find their home after displacement (Demski, 2003) indicate that vision plays an important role in this family, although relatively little is known about their actual visual capabilities.

Genome mining in three species revealed that in addition to a single rod opsin, *RH1*, holocentrids possess several cone opsins: up to two *SWS1* copies, two *SWS2*, up to eight *RH2* paralogs and one *LWS* (Cortesi et al., 2015; Musilova et al., 2019). However, opsin gene expression and microspectrophotometry (MSP) in few species indicate that only a small subset of these opsins may be used in adult fishes (Losey et al., 2003; Musilova et al., 2019). Interestingly, their rod spectral sensitivity correlates with habitat depth, with deeper living holocentrids having shorter spectral sensitivities similar to those found in deep-sea fishes (λ_{max}=480–485 nm), shallower living species having longer sensitivities, comparable to those observed in other shallow-water fishes (λ_{max}=500–507 nm) and individuals living at intermediate depths having sensitivities somewhere in between (λ_{max}=490–495 nm) (Munz and McFarland, 1973; Toller, 1996; Yokoyama and Takenaka, 2004). Furthermore, the holocentrid ancestor is predicted to have had an RH1 sensitive to ∼493 nm λ_{max} suggesting that the family first emerged at intermediate depths (∼100 m or mesophotic depths; Yokoyama and Takenaka, 2004; Yokoyama et al., 2008; Musilova et al., 2019). This putative deeper origin, in addition to their nocturnal lifestyle on the reef and the few species inhabiting the deep sea, therefore make holocentrids particularly interesting for dim-light vision studies.

Using a range of techniques, including high-throughput RNA sequencing (RNA-seq), fluorescence *in situ* hybridization (FISH), photoreceptor spectral sensitivity estimates, and retinal anatomy and topography, we set out to scrutinise the visual system and visual ecology of several species of shallow water holocentrids, with the following two aims in mind: (1) to extend our knowledge about the visual ecology of nocturnal coral reef fishes; and (2) to assess if the holocentrid visual system differs from other nocturnal coral reef fishes because of their atypical ecological and evolutionary ties to deeper habitats.

MATERIALS AND METHODS

Sample collection and ocular tissue preservation

Adult fishes from nine holocentrid species were investigated in the study. Most fishes were collected on the Great Barrier Reef around Lizard Island, Australia, under the Great Barrier Reef Marine Park Permit (G12/35005.1) and the Queensland General Fisheries Permit (140763) using spear guns on SCUBA in 2015 and 2016. Five specimens were obtained from the aquarium supplier Cairns Marine who collects fish from the Northern Great Barrier Reef (Cairns Marine Pty Ltd, Cairns, Australia). Each individual was anaesthetized with an overdose of clove oil (10% clove oil; 40% ethanol; 50% seawater) and killed by decapitation. Eyes were subsequently enucleated, the cornea and lens removed, and the eye cup preserved in different fixative solutions depending on the analysis (see below for details). All experimental procedures were approved by The University of Queensland Animal Ethics Committee (QBI/236/13/ARC/US AIRFORCE and QBI/192/13/ARC).

Histology

One eye of *Sargocentron diadema*, *Neoniphon sammara* and *Myripristis murdjan* was enucleated in daylight conditions and fixed in a solution of 2.5% glutaraldehyde and 2% paraformaldehyde in 0.1 mol l^{-1} phosphate buffered saline (PBS). An extra individual of *S. diadema* was dark adapted for 2 h prior to euthanasia in the dark and one eye was enucleated and fixed as above. The retinas were dissected out of the eye cup and small pieces from different locations (dorsal, temporal, ventral, nasal, central) were post-fixed in 1–2% osmium tetroxide in 0.15 mol l^{-1} PBS, dehydrated through an acetone series, and infiltrated with Epon resin (ProSciTech) using a Biowave tissue processor. Semi-thin transverse sections of the retinas (1 µm) were cut with a glass knife using a Leica EM UC7 Ultramicrotome and stained with an aqueous mixture of 0.5% Toluidine Blue and 0.5% borax. Sections were viewed with a Carl Zeiss Axio Imager compound light microscope and photographed using an Olympus DP70 digital camera. Retinal thickness, photoreceptor layer thickness and rod outer segment length were then measured from the photographs using ImageJ v1.52p (National Institutes of Health, USA). An average of three measurements per parameter were taken.

Transcriptome sequencing, quality filtering and *de novo* assembly

One retina from two Myripristinae (*M. murdjan* and *Myripristis violacea*) and three Holocentrinae species (*S. diadema*, *Sargocentron rubrum* and *Sargocentron spiniferum*) were dissected out of the eye cup and preserved in RNAlater (Thermo Fisher Scientific) at −20°C until further processing. RNA extraction, library preparation and sequencing at the Queensland Brain Institute's sequencing facility followed the protocol outlined in Tettamanti et al. (2019) and Musilova et al. (2019).

Newly sequenced transcriptomes were combined with previously acquired holocentrid transcriptomes from three species: *Myripristis*

berndti (*n*=4), *Myripristis jacobus* (*n*=2) and *N. sammara* (*n*=3) (Musilova et al., 2019), to complete our dataset for opsin gene expression analysis. Transcriptome filtering and *de novo* assembly followed the protocol described in de Busserolles et al. (2017). In brief, raw reads were uploaded to the Genomic Virtual Laboratory (v.4.0.0) (Afgan et al., 2015) on the Galaxy Australia platform (https://usegalaxy.org.au/). The quality of sequences was assessed using FastQC (Galaxy v.0.53) and sequences were filtered using Trimmomatic (Galaxy v.0.32.2) (Bolger et al., 2014) before being *de novo* assembled using Trinity (Galaxy v.0.0.2) (Haas et al., 2013).

Opsin gene mining, phylogenetic reconstruction and expression analyses

Two different strategies were used to mine visual opsin genes from the transcriptomes. First, assembled transcripts were mapped against the opsin gene coding sequences extracted from the genomes of *N. sammara* and *M. jacobus* (Musilova et al., 2019) using the medium sensitivity settings (30% max. mismatch between transcripts) in Geneious v.9.1.5 and v.11.0.2 (www.geneious.com). Because assemblies based on short-read sequences tend to overlook lowly expressed genes and/or may result in hybrid transcripts, a second, raw-read mapping approach was also taken, as described in detail in de Busserolles et al. (2017) and Musilova et al. (2019).

Holocentrid opsin genes were scored for similarity to publicly available opsin sequences using BLASTN (https://blast.ncbi.nlm.nih.gov/Blast.cgi). Their phylogenetic relationship was then confirmed using a reference dataset obtained from GenBank (https://www.ncbi.nlm.nih.gov/genbank/). The combined opsin gene dataset was first aligned in MAFFT v.7.388 (Katoh and Standley, 2013) using the L-INS-I algorithm and default settings in Geneious. jModeltest v.2.1.10 (using AIC for model selection; Ronquist et al., 2012) and MrBayes v.3.2.6 (Ronquist et al., 2012) were then run on the CIPRES platform (Miller et al., 2010) to select the most appropriate model of sequence evolution and to infer the phylogenetic relationship between genes, respectively. We used the GTR+I+γ model, with two independent MCMC searches (four chains each), 10 million generations per run, a tree sampling frequency of 1000 generations, and a burn in of 25% to generate the holocentrid opsin gene consensus tree.

Opsin gene expression was subsequently calculated by mapping the unassembled filtered reads against the extracted coding sequences of each species-specific opsin repertoire (threshold of 2–3% maximum mismatch between reads; read count was normalised to the length of the coding sequence of each opsin), as detailed in de Busserolles et al. (2017) and Tettamanti et al. (2019). The expression of each cone opsin was calculated as the proportion of the total cone opsins expressed or, in the case of the rod opsin, as the proportion of *RH1* compared to the total opsin expression. Because *RH2* paralogs in the Holocentrinae showed high sequence similarity (>96% pairwise identity), *RH2*-specific reads were extracted and sub-mapped against high variability areas (100–200 bp in length). The proportional gene expression of *RH2* paralogs was then re-calculated using normalised read counts from the sub-mapping approach.

Visual pigment maximal absorbance predictions

Maximal absorbance (λ_{max}) of holocentrid visual pigments were estimated by translating opsin gene sequences into amino acid sequences using Geneious and assuming an A1-based chromophore as found in *Sargoncentron spinosissimum* (Toyama et al., 2008). Amino acid sequences were then aligned with bovine rhodopsin (NP_001014890.1) and reference sequences of well-studied model systems with known visual pigment spectral sensitivities using MAFFT (v.7.222) (Katoh et al., 2002). This allowed us to identify holocentrid specific opsin residues corresponding to known tuning and chromophore binding pocket sites according to the protein structure of bovine rhodopsin (Palczewski et al., 2000), and to infer holocentrid pigment spectral sensitivities based on sequence differences to each primary reference sequence: *Oryzias latipes* RH1 (GenBank accession no.: AB180742.1) (Matsumoto et al., 2006); *Oreochromis niloticus* RH2B (JF262086.1) (Parry et al., 2005); *O. niloticus* RH2Abeta (JF262086.1) (Parry et al., 2005); *O. niloticus* SWS2A (JF262088.1) (Parry et al., 2005). For these, we focused on variable amino acid residues either at known tuning sites or at retinal binding pocket sites. Site effects were then inferred either for known substitutions or for substitutions that cause a change in polarity compared to the residue found in the primary reference sequence.

The following sites and effects for the different opsins were considered. RH1: E122M (−7 nm; all species; Yokoyama and Takenaka, 2004), F261Y (+10 nm; *S. spiniferum*, *S. rubrum* and *N. sammara*; Chan et al., 1992), A292S (−10 nm; *S. spiniferum* and *S. rubrum*; Fasick and Robinson, 1998), A295S (−4 nm; *M. jacobus*; Lin et al., 1998; Janz and Farrens, 2001).

SWS2A: I49V (−2 nm; all species; Yokoyama and Tada, 2003), A164S (−2 nm; *S. spiniferum*, *M. violacea*, *M. murdjan*, *M. berndti*, *M. jacobus*; Yokoyama and Tada, 2003), A269T (+6 nm; all species except *M. jacobus*; Yokoyama and Tada, 2003), L216F (−4/−8 nm upper/lower limit; all species). L216F in combination with M205I most likely explain the 8 nm difference between *O. niloticus* SWS2A (456 nm λ_{max}; Parry et al., 2005) and *Pseudochromis fuscus* SWS2Aβ (448 nm λ_{max}; Cortesi et al., 2015). Since all holocentrid sequences contained a methionine at residue 205, and as it is unclear whether L216F alone, M205I alone, or both substitutions together contribute to the 8 nm shift, we calculated upper and lower limit λ_{max} values, accounting for a 4 and an 8 nm blue shift, respectively, caused by L216F.

RH2A (only Holocentrinae): F60I/M/L/V (0/−1 nm upper/lower limit; all species; Yokoyama and Jia, 2020), Y74F (0/−1 nm; all species; Yokoyama and Jia, 2020), V255I (0/−1 nm; all species except *N. sammara* RH2A-1, *S. spiniferum* RH2A-2 and RH2A-3; Yokoyama and Jia, 2020), M259F/V (0/−1 nm; all species; Yokoyama and Jia, 2020), G273A (0/−1 nm; all species; Yokoyama and Jia, 2020). Substitutions at these sites are part of a site effect complex shown to cause strong red shifts in several teleost lineages compared with their ancestors (+21 nm; Yokoyama and Jia, 2020). However, the bulk of this shift is caused by the substitutions Y96T, Q122E and C213F, whereas the other substitutions may cause much smaller individual effects, if any. The substitutions observed at these five sites in Holocentrid RH2A opsins are inversions (either of the amino acids involved or of the polarity of substituted amino acids) and were therefore tentatively hypothesized to cause effects opposite to those described by Yokoyama and Jia (2020). For lower limit calculations we thus hypothesized each site, where present in the sequence, to cause a −1 nm blue shift.

RH2B (only Myripristinae): Y96T/Q122E/C213I (+20 nm; all species; Yokoyama and Jia, 2020), I49C/S and S109G combined (+8 nm; all species; Luehrmann et al., 2019).

Fluorescence *in situ* hybridization (FISH)

After dark adaptation for 1 hour, the eyes of two *N. sammara* and one *M. berndti* were enucleated and prepared following previously

Journal of Experimental Biology (2021) 224, jeb233098. doi:10.1242/jeb.233098

described methods (Barthel and Raymond, 2000). Dual-labelling FISH was performed on whole mount retinas or quadrants of retina for very large retinas following standard protocols (Raymond and Barthel, 2004; Allison et al., 2010; Dalton et al., 2014, 2015). In brief, RNA was reverse transcribed using the High Capacity RNA-to-cDNA kit (Applied Biosystems). cDNA was then used to generate the probe template by standard PCR using the MyTaq™ HSRED DNA Polymerase (Bioline) and opsin specific primers (listed in Table S1) designed to bind to the 3′ untranslated region (3′ UTR) (*RH2A-1* and *RH2A-2* in *N. sammara*) or the coding sequence (*SWS2A* in *N. sammara*, *SWS2A* and *RH2B* in *M. berndti*). Probes were then labelled with DIG or Fluorescein (Roche DIG/Fluorescein RNA Labeling Mix, Sigma Aldrich), tagged with Alexa Fluor 594 or 488 dyes (Invitrogen), and the signal enzymatically augmented with sequential tyramide signal amplification (TSA amplification kits, Invitrogen). Finally, retinas or retinal pieces were mounted, photoreceptor side up, on coverslips in 70% glycerol in PBS.

For visualization of labelled opsin genes, multi-channel scans for each dual-labelled opsin pair were performed using a spinning-disk confocal microscope consisting of a Nikon Ti-E (Nikon Instruments Inc.) equipped with a Diskovery spinning-disk platform (Spectral Applied Research), and Zyla 4.2 sCMOS cameras (Andor). NIS Elements (Nikon Instruments Inc.) were used to perform multi-channel imaging with a CFI Plan Apochromat VC 20x objective (NA 0.75, WD 1.00 mm), and a water immersion CFI Apo Lambda S 40× objective (NA 1.25, WD 0.18 mm) for high resolution images. All scans were exported as TIFs and further processed (merging of colour channels, adjusting of brightness) with ImageJ v.1.8.0_66 (National Institutes of Health, USA).

Preparation of retinal whole mounts

Eyes were fixed in 4% PFA in 0.1 mol l^{-1} PBS (pH=7.4) for 48 h. Retinal whole mounts were then prepared according to standard protocols (Stone, 1981; Coimbra et al., 2006; Ullmann et al., 2011). The orientation of the retina was kept by referring to the position of the falciform process that ends ventrally for Holocentrinae and naso-ventrally for the Myripristinae. Each retina was bleached overnight at room temperature in a solution of 3% hydrogen peroxide in 0.1 mol l^{-1} PBS.

For photoreceptor analysis, retinas were whole mounted (photoreceptor layer up) in 100% glycerol on a microscope slide. For ganglion cell analysis, the retinas were whole mounted, ganglion cell layer facing up, on a gelatinised slide, left to dry overnight in formalin vapour to improve fixation and cell differentiation (Coimbra et al., 2006, 2012) and stained in 0.1% Cresyl Violet (Coimbra et al., 2006). Possible shrinkage during staining was considered negligible and if present confined to the retinal margins, since the retinal whole mount remained attached to the slide throughout the staining process (Coimbra et al., 2006).

Distribution of the different neural cell types across the retina

Different types of analyses were performed for high-density cell types (that is, single cones, double cones and ganglion cells) and low-density cell types (triple cones). Following the protocols described in de Busserolles et al. (2014a,b), topographic distribution of single cones, double cones, total cones and ganglion cells were assessed using the optical fractionator technique (West et al., 1991) modified by Coimbra et al. (2009, 2012). Briefly, using the parameters listed in Table S2 and a 63× oil objective (NA 1.40) mounted on a compound microscope (Zeiss Imager.Z2) equipped with a motorised stage (MAC 6000 System, Microbrightfield, USA), a digital colour camera (Microbrightfield) and a computer running StereoInvestigator software (Microbrightfield), cells were randomly and systematically counted. The counting frame and grid size were chosen carefully to maintain the highest level of sampling (~200 sampling sites) and achieve an acceptable Schaeffer coefficient of error (CE <0.1; Glaser and Wilson, 1998).

Single cones and double cones were easily distinguished (Fig. 1) and counted separately and simultaneously using two different markers to generate data for single cones alone, double cones alone, and the two cell types combined (total cones). Owing to the low number of single cones present in the retinas of all holocentrids, the analysis for the single cones was repeated using a larger counting frame (Table S2).

In Holocentrinae, ganglion cells were arranged in a single layer in the ganglion cell layer. However, in Myripristinae, several ganglion cells were displaced and present in the inner nuclear layer. Since it was not always possible to confidently identify the ganglion cells present in the inner nuclear layer from the other cell types (amacrine and bipolar cells), only ganglion cells present in the ganglion cell layer were counted in this study. Furthermore, only ganglion cells were counted as they were easily distinguished from the other cell types present in the ganglion cell layer (amacrine and glial cells) using cytological criteria alone (Hughes, 1975; Collin and Collin, 1988).

Topographic maps were constructed in R v.2.15.0 (R Foundation for Statistical Computing, 2012) with the results exported from the Stereo Investigator Software according to Garza-Gisholt et al. (2014). The Gaussian kernel smoother from the Spatstat package (Baddeley and Turner, 2005) was used and the sigma value was adjusted to the grid size.

The distribution of the triple cones was mapped from one retina of *S. rubrum* using the Neurolucida software (MicroBrightField). The outline of the retinal whole mount was digitized using a 5× objective (numerical aperture, 0.13). The entire retina was then scanned in contiguous steps using a 20× objective (numerical aperture, 0.8), and each triple cone was marked. Results were exported from the Neurolucida software, and a dot map representing the location of each triple cone was constructed in R using a customized script based on Garza-Gisholt et al. (2014).

Spatial resolving power

The upper limit of the spatial resolving power (SRP) in cycles per degree was estimated for each individual using the peak density of ganglion cell (PDG in cells mm^{-1}) as described by Collin and Pettigrew (1989). Briefly, the angle subtending 1 mm on the retina (angle α) can be calculated as follows:

$$\alpha = \arctan(1/f), \quad (1)$$

where f, the focal length, is the Matthiessen's ratio (i.e. the distance from the centre of the lens to the retina; Matthiessen, 1882) times the radius of the lens. While in most teleosts the Matthiessen's ratio is close to 2.55, in holocentrids it is between 2.1 and 2.2 (McFarland, 1991). Accordingly, we used a ratio of 2.15 in this study. Knowing α, the PDG and the fact that two ganglion cells are needed to distinguish a visual element from its neighbour, the SRP in cycles per degree (cpd) can be calculated as follows:

$$\mathrm{SRP} = (\mathrm{PDG}/\alpha)/2. \quad (2)$$

Journal of Experimental Biology (2021) 224, jeb233098. doi:10.1242/jeb.233098

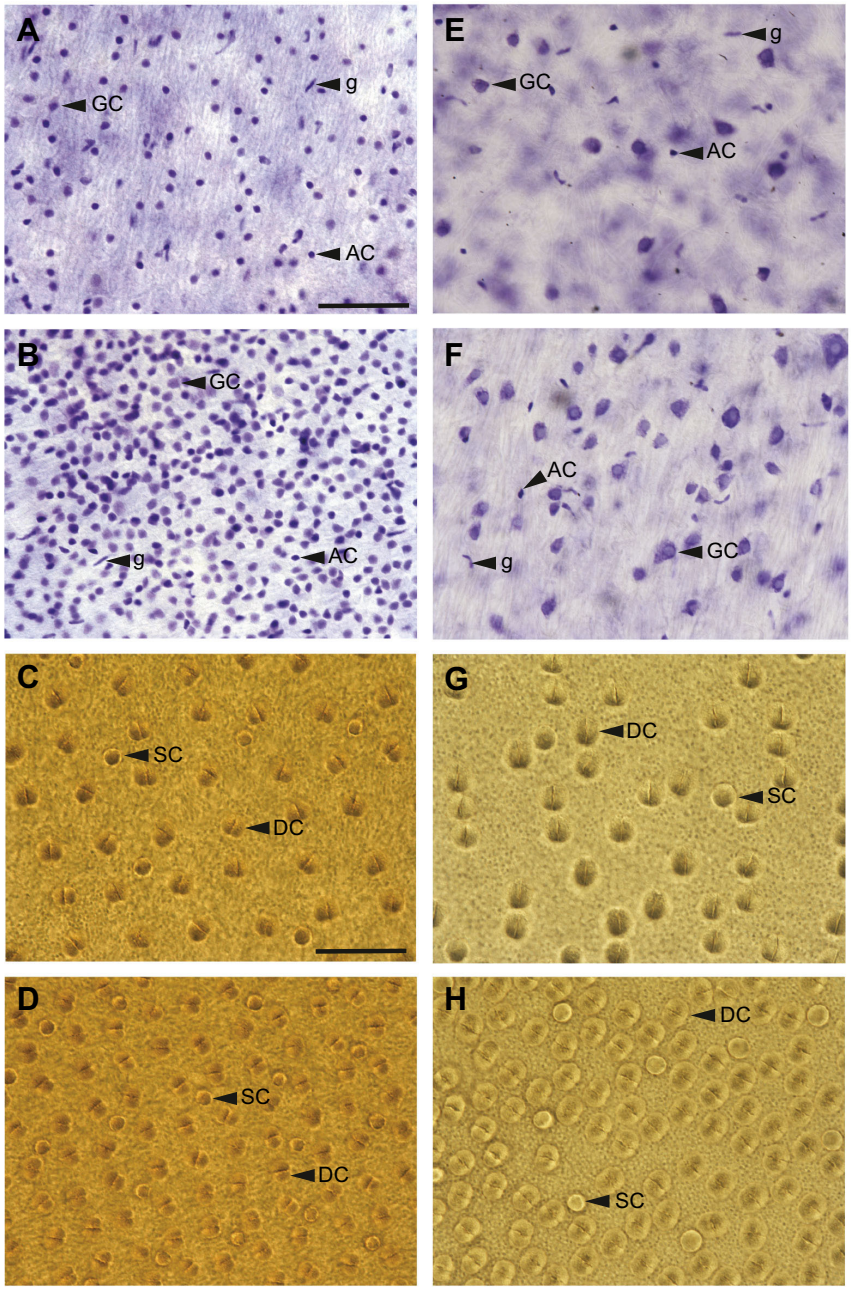

Fig. 1. Whole mount views of the retinas of two holocentrid species, *Neoniphon sammara* and *Myripristis berndti*. Ganglion cell layer (A,B,E,F) and cone photoreceptor layer (C,D,G,H) in *Neoniphon sammara* (A–D) and *Myripristis berndti* (E–H). For each species and cell type, a picture was taken in a low-density area (A,C,E,G) and a high-density area (B,F,D,H) for comparison. GC, ganglion cell; AC, amacrine cell; g, glial cell; SC, single cone; DC, double cone. Scale bars: 50 µm.

RESULTS

Anatomy of the retina

Holocentrids have a typical vertebrate retina organised in several layers: photoreceptor, outer nuclear, inner nuclear and ganglion cell layer (Fig. 2A,C). However, compared to most vertebrates that possess a single photoreceptor layer containing both rod and cone cells, holocentrids possess a multibank retina composed of one layer of cones and several layers of rods. In the three species investigated (from three different genera and the two subfamilies) this multibank organisation was found across the entire retina (Fig. S1). However, the number of rod banks varied in different areas of the retina and between species (Fig. 2, Fig. S1). Up to six and seven banks could be identified in *N. sammara* and *S. diadema* (Holocentrinae), respectively, while in *M. murdjan* (Myripristinae) up to 17 banks were observed. The highest number of banks in the Holocentrinae was found in the temporal and central areas whereas in *M. murdjan* the highest number of banks was found in the ventral area (Fig. S1). Indicative of a higher rod photoreceptor density, the outer nuclear layer (ONL) in *M. murdjan* also showed an increased thickness compared to the ONL in Holocentrinae (Fig. 2). In all three species, the rod outer segment length appeared to be uniform across all banks but varied between species. Overall the higher the numbers of banks, the shorter were the outer segments (~15 µm in *M. murdjan*, ~21 µm in *S. diadema* and ~31 µm in *N. sammara*). However, at least for *S. diadema*, the width of the outer segment seemed to increase from layer to layer, with the first layer (B1, most scleral layer) having the thinnest rods (Fig. 2B). Consequently, in *S. diadema*, the first layer of rods (B1) had the highest density of cells and the last layer (B7) had the lowest. It is notable that for several sections from all three species, the rod

Journal of Experimental Biology (2021) 224, jeb233098. doi:10.1242/jeb.233098

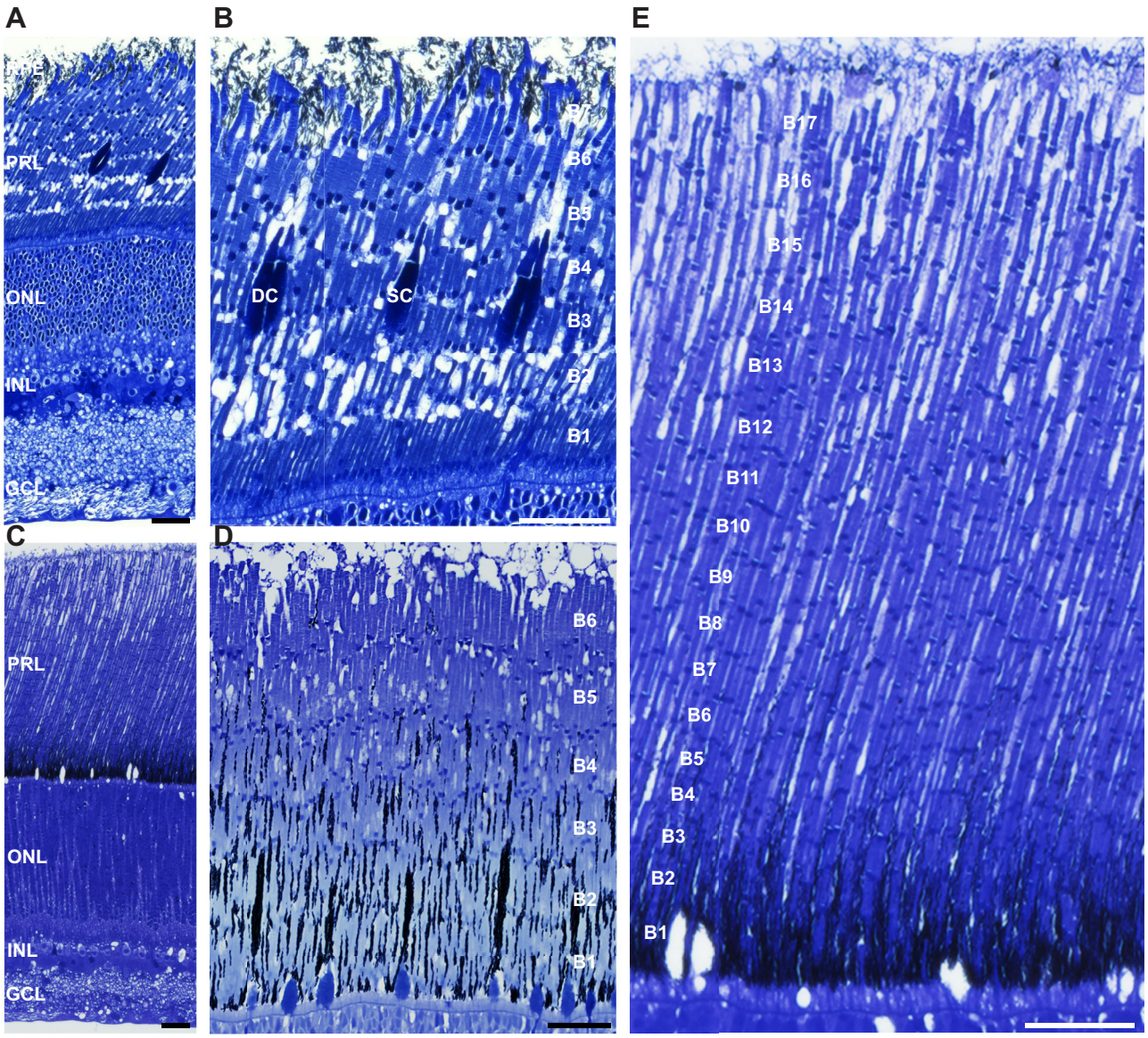

Fig. 2. Transverse light microscopy sections through the multibank retina of three species of holocentrids in different light conditions. (A,B) Dark-adapted *Sargocentron diadema*. (D) Light-adapted *Neoniphon samara*. (C,E) Light-adapted *Myripristis murdjan* (C,E). A and C are low magnification images showing all the retinal layers in a representative from each subfamily, Holocentrinae (*S. diadema*, A) and Myripristinae (*M. murdjan*, C). RPE, retinal pigment epithelium; PRL, photoreceptor layer; ONL, outer nuclear layer; INL, inner nuclear layer; GCL, ganglion cell layer. (B,D,E) High magnification of the photoreceptor layer showing the maximum number of rod banks (B1–B17) in the three species studied. DC, double cone, SC, single cones. Scale bars: 25 µm.

nuclei in the ONL were arranged in vertical lines, as illustrated for *M. murdjan* in Fig. 2C.

Although rod-dominated, three types of cones (single, double and triple) were also found in the retinas of holocentrids (Fig. 3A). Double cones were the most frequent type, followed by single cones, while triple cones were rarely found. In *Myripristis* spp., double and single cones were not organised in a regular array or mosaic, but instead were arranged randomly throughout the retina (Fig. 1). In Holocentrinae, cone arrangements varied in different parts of the retina. In general, double cones were organised in regular rows, except in the temporal retina where the arrangement was more squared (i.e. double cones were positioned at an angle) and in the central retina where there was no apparent organisation. Single cones appeared evenly spread out throughout the retina although no obvious general pattern was observed, except in the nasal retina of *N. sammara* where they were arranged in a square pattern. When present, single cones in Holocentrinae were always placed in the middle of four double cones, as seen in the classic teleost square mosaic (Fig. 1C,D).

The holocentrid retina also showed clearly discernible photoreceptor and retinal pigment epithelium (RPE) retinomotor movements. In the light-adapted state (Fig. 2D,E), the cones and the melanin pigment granules within the RPE were positioned in the most vitreal part of the photoreceptor layer at the level of the first rod bank (Fig. 2D,E). Conversely, in the dark-adapted state, cones were positioned at the level of the third rod bank and the melanin pigment granules migrated all the way to the top of the last rod layer (Fig. 2B).

Visual opsin genes and their expression

Transcriptomes from eight holocentrid species (four species per subfamily) showed that they predominantly express one rod opsin and either two (Myripristinae) or three cone opsins (Holocentrinae)

Journal of Experimental Biology (2021) 224, jeb233098. doi:10.1242/jeb.233098

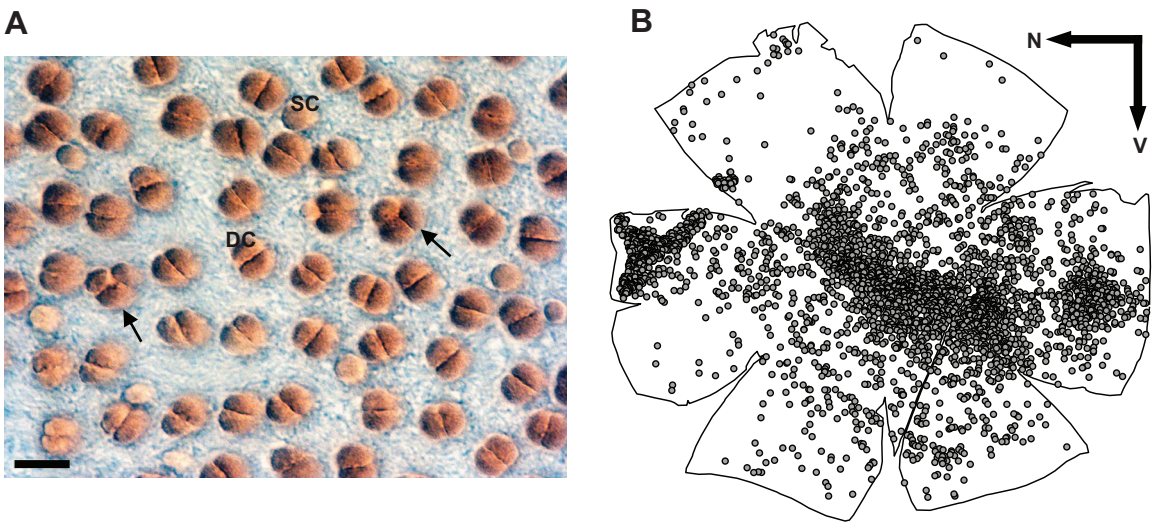

Fig. 3. Presence of triple cones in the Holocentridae *Sargocentron rubrum*. (A) Whole mount view of the photoreceptor layer showing the different types of cone photoreceptors and the presence of triple cones (black arrow). SC, single cone; DC, double cone. Scale bar: 15 µm. (B) Distribution of the triple cones across the retina. Each dot represents one triple cone. Black arrows indicate the orientation of the retina. N, nasal; V, ventral.

within their retinas. Phylogenetic reconstruction identified these opsins to be *RH1* (rod opsin; dim-light vision), *SWS2A* (blue-sensitive), and either *RH2B-1* or two *RH2A* paralogs (*RH2A-1* and *RH2A-2*; blue-green-sensitive) for Myripristinae and Holocentrinae, respectively. We were also able to extract a partial *RH2B-2* sequence from the *M. murdjan* transcriptome and found evidence for a third *RH2A-3* copy in *S. spiniferum* (Fig. 4A).

Quantitative opsin gene expression was highly similar within subfamilies with detailed values for each individual and species listed in Table S3. Opsin gene expression was strongly rod dominated; *RH1* expression made up 99.45±0.08% (mean±s.e.m.) of the total opsin gene expression in Myripristinae and 94.92±0.97% in Holocentrinae. Within cone opsins, *SWS2A* (Myripristinae: 6.83±0.92%, Holocentrinae: 5.12±0.16%) showed much lower expression compared to *RH2* genes (Myripristinae *RH2B*: 93.17±0.92%, Holocentrinae *RH2A-1*: 45±3.90% and *RH2A-2*: 49.70±3.91%). Finally, while *RH2B-2* in *M. murdjan* was expressed at levels that were too low to reconstruct its full coding sequence, *RH2A-3* in *S. spiniferum* made up ∼1.1% of its cone opsin expression (Fig. 4B; Table S3).

Fluorescence *in situ* hybridization

FISH was performed on the retinas of two holocentrid species, *N. sammara* (Holocentrinae) and *M. berndti* (Myripristinae). In both species, *SWS2A* expression was limited to single cones while *RH2* opsins (*RH2B-1* for *M. berndti*; *RH2A-1* and *RH2A-2* for *N. sammara*) were expressed in the double cones only (Fig. 5). Moreover, in *N. sammara*, the two *RH2A* paralogs were co-expressed in both members of the double cones (Fig. 5). These expression patterns were consistent throughout the retina of each respective species.

Visual pigment maximal absorbance predictions

Since spectral sensitivity information for Holocentridae was sparse in the literature, especially for cones, and since transcriptomic data revealed the presence of several *RH2* genes in Holocentrinae, we estimated the maximum absorbance (λ_{max}) of each opsin protein based on their amino acid sequence for the eight species from which retinal transcriptomes were available (Table 1). Predicted values were then compared with measured spectral sensitivities from the literature (Munz and McFarland, 1973; McFarland, 1991; Toller, 1996; Losey et al., 2003). Estimated λ_{max} of holocentrid RH1 pigments ranged from 491 nm in *M. jacobus* to 505 nm in *N. sammara*. RH1 estimations in all other species fell within this range with a predicted λ_{max} value of 495 nm. With the exception of *M. violacea* (λ_{max} MSP: 499 nm), these predictions fit well with previous MSP measurements of holocentrid rods (Munz and McFarland, 1973; McFarland, 1991; Toller, 1996; Losey et al., 2003).

Estimated spectral sensitivities for the SWS2A pigments ranged from 442/448 nm (lower/upper limit) in *M. jacobus* to 450/456 nm in *N. sammara*, *S. diadema* and *S. rubrum*. For *S. spiniferum*, *M. violacea*, *M. murdjan* and *M. berndti*, SWS2A λ_{max} were estimated at 448/454 nm. Compared with the available single cone MSP measurements (Losey et al., 2003), these predictions are all slightly long-wavelength shifted (λ_{max} MSP: *M. berndti*, 443/453 nm; *N. sammara*, 446 nm) (Table 1).

For all Myripristinae, RH2B-1 was estimated to be maximally sensitive at 500 nm. In *M. berndti*, this estimate was similar to the lower limit of the double cone spectral sensitivities measured by MSP (mean±s.d.: 506±2.4 and 514±1.4 nm) (Losey et al., 2003). Moreover, while MSP measurements suggested the presence of two spectrally different double cone types, the retinal transcriptome of *M. berndti* only contained a single *RH2* opsin gene. In Holocentrinae, there was no or only very little difference (±1 nm) in the λ_{max} estimates of the different RH2A paralogs (λ_{max}=513–514/518 nm). These predictions were comparable to the *N. sammara* double cone λ_{max} measured by MSP (λ_{max}=512±3.0 nm; Losey et al., 2003) (Table 1).

Topographic distribution of ganglion cells and cone photoreceptors

The topographic distribution of ganglion cells and cone photoreceptors (double, single and total cones) was investigated in four Myripristinae and five Holocentrinae species from three different genera: *Myripritis*, *Neoniphon* and *Sargocentron*. Overall, while individuals and species within the same subfamily showed similar distributions of ganglion and cone photoreceptor cells (Figs S2

Journal of Experimental Biology (2021) 224, jeb233098. doi:10.1242/jeb.233098

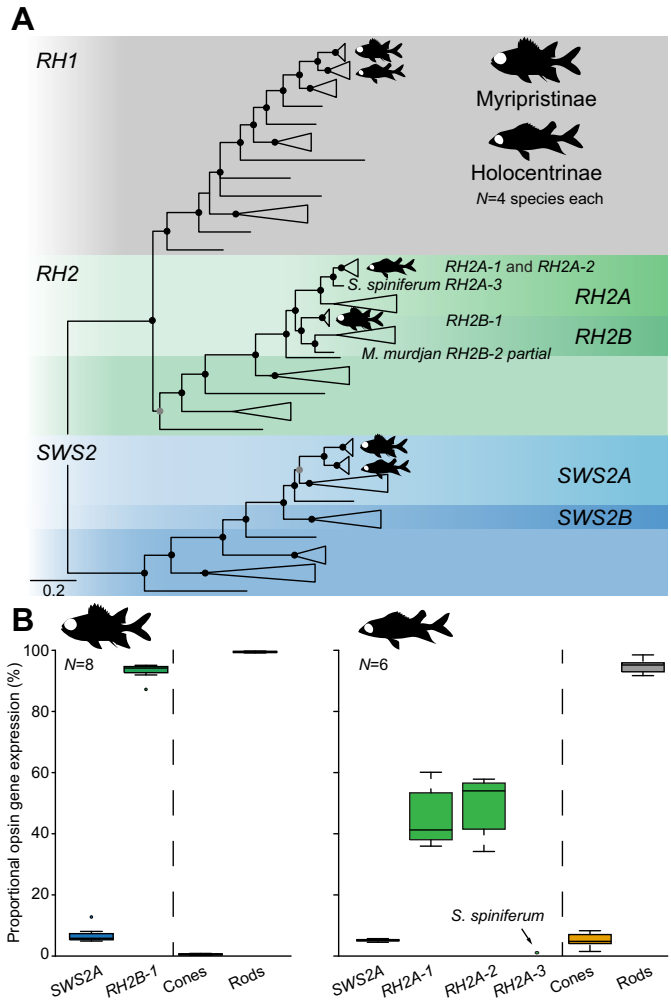

Fig. 4. Vertebrate visual opsin gene phylogeny and opsin gene expression in Holocentridae. (A) Holocentrid retinal transcriptomes contained one rhodopsin 1 (rod opsin, *RH1*), one short-wavelength sensitive 2 (*SWS2A*), and multiple mid-wavelength-sensitive rhodopsin-like 2 (*RH2*) cone opsins. Black and grey circles indicate Bayesian posterior probabilities >0.9 and >0.75, respectively. Note that a third *RH2A-3* paralog was found in *Sargocentron spiniferum*, and a partial second *RH2B-2* paralog was reconstructed from the *Myripristis murdjan* transcriptome. (B) Per-subfamily mean of the proportional opsin gene expression. The box indicates the second and third quartiles, the central line is the median and the whiskers indicate the first and fourth quartiles of the data. Details including individual expression levels, transcriptome read counts and SRA accession numbers are given in Table S3.

and S3) retinal topographies did differ between subfamilies. The retinal topography of each cell type for one representative species per genus is shown in Fig. 6 and detailed retinal topographies for the remaining species are provided in Fig. S3.

Ganglion cell distribution and spatial resolving power

The ganglion cell distribution revealed subfamily specific specialisations (Fig. 6). Holocentrinae had a well-defined area temporalis that weakly extended along the horizontal meridian but did not reach the nasal area of the retina. Myripristinae, on the other hand, had a very large area centralis with a peak density in the ventral–temporal part of the retina. In addition, *M. berndti* and *M. murdjan* also had a horizontal streak (Fig. S3). The subfamilies also differed in their ganglion cell numbers and densities (Table 2). Holocentrinae had a higher total number of ganglion cells compared with Myripristinae, with an average of 830,000 cells and 580,000 cells, respectively. Ganglion cell peak densities were also much higher in Holocentrinae compared with Myripristinae, with densities ranging from 9510 to 23,786 cells mm^{-2} and 2150 to 5990 cells mm^{-2}, respectively. Consequently, although Myripristinae usually had bigger lenses (Table S2), Holocentrinae had higher visual acuity estimates. Most Holocentrinae had an estimated spatial resolving power (SRP) of around 7 cycles per degree with the highest acuity recorded for *N. sammara* at 11 cycles per degree while all Myripristinae had an estimated SRP of around 4 cycles per degree (Table 2).

Total cone distribution

Similarly to the ganglion cell distribution, total cone topography differed between subfamilies (Fig. 6). Myripristinae had a strong horizontal streak, slightly oblique in orientation, with a peak cell density in the central to temporal area. Holocentrinae, on the other hand, had two areas located temporally and nasally, as well as a weak horizontal streak. Moreover, their peak cell density was found in the temporal area (Fig. S3) with the exception of *S. rubrum* where the peak cell density was found nasally. *M. pralinia* had an intermediate specialisation (one area and a weak horizontal streak, Fig. S3) between the one found for the remaining Myripristinae (Fig. S3) and the Holocentrinae (Fig. S3). Interestingly, for all Myripristinae, peak cell densities and topography patterns of total cone photoreceptors did not match the ones found for ganglion cells (Fig. 3, Fig. S3). In Holocentrinae, peak cell densities of total photoreceptors and ganglion cells matched pretty well even though the topography patterns were slightly different between cell types; the ganglion cell pattern was mainly defined by an area temporalis while the total photoreceptor pattern was characterised by two areas and a weak horizontal streak. Similarly to the ganglion cell numbers, Holocentrinae had more cones than Myripristinae with numbers ranging from 586,815 to 984,127 cells and 308,075 to 637,051 cells, respectively (Table 3).

Double cone distribution

Double cones were the main cone photoreceptor type found in the holocentrid retina, accounting for ∼87% of all cones (Table 3). As a result, the double cone topography matched the total cone topography for all species (Fig. 6, Fig. S3).

Single cone distribution

Single cones only accounted for ∼13% of the total cone population in the holocentrid retina (Table 3). The difference in single cone topography between the two subfamilies was the most pronounced of all neural cell types (Fig. 6, Fig. S3). In Myripristinae, the strong streak seen in the double cone topographies nearly disappeared and was replaced by a small area temporalis. In Holocentrinae, the single cone pattern was quite similar to the double cone patterns, with the two areas (temporal and nasal) and a weak streak. However, single cones were also more numerous in the ventral part, and interspecific variability was greater compared with the double cones in this subfamily (Fig. S3). With the exception of *N. sammara*, for which the single cone peak density was in the nasal area while the double cone peak density was in the temporal part, all Holocentrinae species had their single and double cone peak densities in the temporal part of the retina.

Ratio of double to single cones

The mean double to single cone ratio (DC/SC ratio) across the retina varied between species from 4:1 in *S. rubrum* to 9:1 in *M. berndti*,

Journal of Experimental Biology (2021) 224, jeb233098. doi:10.1242/jeb.233098

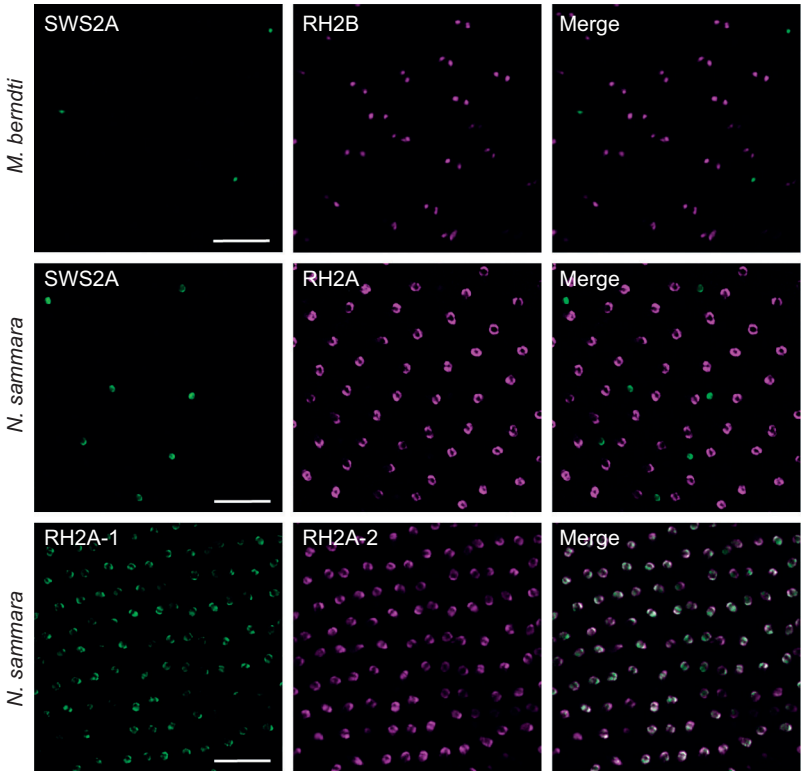

Fig. 5. Opsin expression in single and double cones revealed by fluorescence *in situ* hybridization (FISH) in whole mount retinas of *Myripristis berndti* and *Neoniphon sammara*. Images reveal the expression patterns of *SWS2A* (green) in single cones and *RH2* (magenta) in double cones. In *N. sammara* (bottom panel), the two copies of the *RH2* genes (*RH2A-1* and *RH2A-2*) are co-expressed in each member of every double cone. Scale bars: 50 µm.

with most species having a ratio of 7:1 (Table 3). The topography of DC/SC ratio was similar for all species with a higher DC/SC ratio in the dorsal part of the retina (Fig. 6, Fig. S3).

Triple cones

Triple cone density and distribution was assessed for one individual of *S. rubrum*, the species for which the most triple cones were observed across the retina. Triple cones for this individual only represented 0.5% of the total cone population. While triple cones were present throughout most of the retina, they were more concentrated along the horizontal meridian, in a similar pattern to the total cone distribution (Fig. 3).

DISCUSSION

The holocentrid multibank retina

The most striking feature of the holocentrid visual system is its multibank retina. While anecdotally mentioned by McFarland (1991), the multibank aspect of the holocentrid retina was not

Table 1. Summary of holocentrid photoreceptor spectral sensitivities measured using ESP and MSP data from previous studies and predicted using amino acid sequences (this study)

	Rods		Single cones		Double cones	
Species	Measured	Estimated	Measured	Estimated	Measured	Estimated
Myripristis berndti	493[1,2], 495[3]	495	443, 453[3]	448–454	506, 514[3]	500
Myripristis violacea	499[2]	495	–	448–454	–	500
Myripristis murdjan	–	495	–	448–454	–	500
Myripristis jacobus	–	491	–	442–448	–	500
Neoniphon sammara	502[1–3]	505	446[3]	450–456	512[3]	513–518 514–518
Neoniphon aurolineatus	481[1,2]	–	–	–	–	–
Neoniphon argentus	502[1,2]	–	–	–	–	–
Sargocentron spiniferum	490[1,2]	495	–	448–454	–	513–518 513–518 514–518
Sargocentron diadema	490[1], 491[2]	495	–	450–456	–	513–518 513–518
Sargocentron rubrum	–	495	–	450–456	–	513–518 513–518
Sargocentron punctatissimum	494[2], 495[1]	–	–	–	–	–
Sargocentron microstoma	494[2]	–	–	–	–	–
Sargocentron tiere	489[1], 490[2]	–	–	–	–	–
Sargocentron xantherythrum	490[3]	–	447[3]	–	509, 516[3]	–
Holocentrus adscensionis	500[4]	–	440[3]	–	515, 520[3]	–

[1]Munz and McFarland, 1973; [2]Toller, 1996; [3]Losey et al., 2003; [4]McFarland, 1991. Note that *N. sammara*, *S. spiniferum*, *S. diadema* and *S. rubrum* express two or three RH2A paralogs in double cones, therefore, a sensitivity estimation for each paralog is provided.

Journal of Experimental Biology (2021) 224, jeb233098. doi:10.1242/jeb.233098

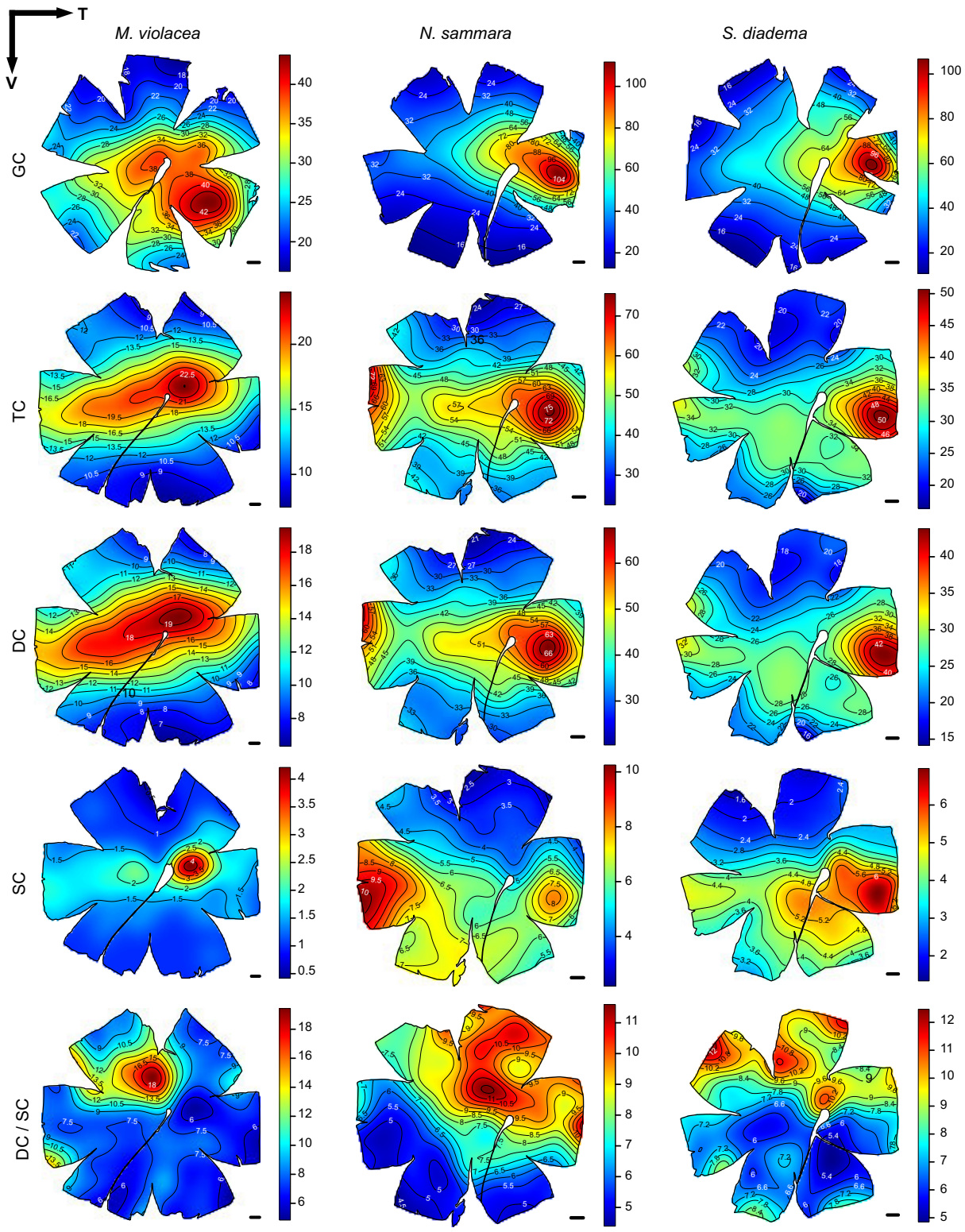

Fig. 6. Topographic distribution of the different neural cells in the retina of three representative species from three different genera of Holocentridae, *Myripristis violacea*, *Neoniphon sammara* and *Sargocentron diadema*. GC, ganglion cells; TC, total cones; DC, double cones; SC, single cones; DC/SC, ratio of double to single cones. The black lines represent iso-density contours and values are expressed in densities ×10^2 cells mm^{-2}, except for DC/SC. The black arrow indicates the orientation of the retinas. T, temporal; V, ventral. Scale bars: 1 mm.

properly assessed or described. Multibank retinas are usually found in teleost species that live in dim-light conditions, mainly deep-sea fishes (Wagner et al., 1998) and a few nocturnal shallow or freshwater species (Gordon et al., 1978; Shapley et al., 1980; Hess et al., 1998; Omura and Yoshimura, 1999; Bozzano, 2003; Meyer-Rochow and Coddington, 2003; Omura et al., 2003; Taylor and Grace, 2005; Taylor et al., 2015). Within the shallow-water representatives, two are reef associated: the moray eel, *Muraena*

Journal of Experimental Biology (2021) 224, jeb233098. doi:10.1242/jeb.233098

Table 2. Summary of the ganglion cell data using the optical fractionator method in several species of holocentrids

Species	ID	Total number	Peak density (cells mm^{-2})	Lens ⌀ (mm)	SRP (cpd)
Myripristis berndti	A	563,622	2150	8.5	3.71
	B	537,435	2200	9.4	4.15
Myripristis violacea	A	649,936	4488	6.5	4.11
	B	627,788	5990	5.3	3.89
Myripristis murdjan	A	544,548	2800	8.8	4.38
Myripristis pralinia	A	564,032	2475	8.3	3.89
Neoniphon sammara	A	1,032,300	22,248	5.5	7.77
	B	976,302	23,786	6.7	9.76
Sargocentron spiniferum	A	814,941	10,399	7.1	6.83
	B	829,733	11,732	7.2	7.36
Sargocentron diadema	A	755,478	20,624	5.1	6.95
	B	747,013	21,040	5.0	6.88
Sargocentron rubrum	A	744,565	9510	8.0	7.35
Sargocentron violaceum	A	711,111	10,754	6.6	6.46

⌀, diameter; SRP, spatial resolving power; cpd, cycles per degree.

helena, and the conger eel, *Ariosoma balearicum* (Hess et al., 1998). Therefore, the presence of a multibank retina in Holocentridae, a nocturnal coral reef fish family with a strong link to the deep sea (Yokoyama et al., 2008; Greenfield et al., 2017), while certainly unusual, may not be surprising.

Similarly to the majority of teleosts with multibank retinas, rods in holocentrids are organised in well-defined banks. In other species the number of banks may vary in different parts of the retina (Locket, 1985) and/or during ontogeny with banks added as fishes grow (Fröhlich and Wagner, 1998; Omura et al., 2003). While the number of banks seems to vary across the holocentrid retina, it is currently not known if banks are added ontogenetically, and at what stage/age the multibank starts to develop in the first place. Shand (1994b), studied the gross retinal structure of holocentrid larvae at settlement stage (i.e. after metamorphosis) and did not report a multibank retina. This suggests that the extra banks are added later, although a more in-depth study of the development of the holocentrid retina is needed to confirm this.

The number of banks found in the holocentrid retina (6–17) is high compared with other species. All shallow and freshwater species and most deep-sea fishes with multibank retinas only have 2–6 banks. To date, only five deep-sea species are known to possess more than six banks, with a record of 28 banks found in the deep-sea bigeye smooth-head, *Bajacalifornia megalops* (Locket, 1985; Denton and Locket, 1989; Fröhlich and Wagner, 1998; Landgren et al., 2014). However, in *B. megalops*, this extremely high number of banks is constrained to the fovea while the rest of the retina has 2–3 banks (Locket, 1985). Therefore, holocentrids, and especially species from the genus *Myripristis*, are part of a small group of fishes with an exceptionally high number of rod banks. Since the three species analysed in this study are shallow-water representatives, a comparison with the retinal structure of deep-sea holocentrids would be of particular interest.

Although common in deep-sea fishes, the function of multibank retinas is still poorly understood. Amongst the several theories put forward, two non-mutually exclusive hypotheses are common: (1) multibank retinas enhance the sensitivity of the eye by increasing the density and length of the rods (Wagner et al., 1998; Warrant et al., 2003); (2) they enable rod-based colour discrimination by changing the light chromatically as it passes through the different banks (Denton and Locket, 1989). Support for either hypothesis is lacking, mostly because of the difficulty to access live deep-sea specimens to conduct physiological and/or behavioural experiments. Therefore, holocentrids may offer an ideal model to address these questions as they can be readily accessed and trained in captivity. Their large eyes (Schmitz and Wainwright, 2011), short focal length (McFarland, 1991), rod-dominated retina (this study), extremely high *RH1* expression compared to other coral reef fishes [i.e. >95% in holocentrids (this study) versus 50–70% in damselfishes (Stieb et al., 2016, 2019) and diurnal apogonids (Luehrmann et al., 2019)], and their rod spectral sensitivity tuned to their respective depth range (Toller, 1996), indicate a visual system well-adapted to dim-light vision and a need for increased sensitivity. Therefore, multibank retinas in holocentrids are likely to contribute toward enhancing the overall light sensitivity of their eyes. However, a use in colour vision during crepuscular hours or at night is also a possibility (Denton and Locket, 1989).

Table 3. Summary of the photoreceptor data using the optical fractionator method in several species of holocentrids

Species	ID	Total DC	Peak DC	Total SC	Peak SC	Total PR	Ratio DC/SC	% DC	% SC
Myripristis berndti	D	571,431	3733	65,620	844	637,051	9	90	10
Myripristis violacea	B	460,728	2355	58,117	988	518,845	8	89	11
	C	476,597	2666	62,673	1500	539,270	8	88	12
Myripristis murdjan	B	394,286	2110	59,884	1121	454,170	7	87	13
	C	358,006	1167	52,674	655	410,680	7	87	13
Myripristis pralinia	A	259,800	1178	48,275	644	308,075	5	84	16
Neoniphon sammara	A	864,973	7337	119,154	1242	984,127	7	88	12
	C	812,840	8047	117,855	1183	930,695	7	87	13
Sargocentron spiniferum	A	749,341	3777	110,180	678	859,521	7	87	13
Sargocentron diadema	C	580,245	5555	79,056	1344	659,301	7	88	12
	D	522,126	5999	64,689	1433	586,815	8	89	11
Sargocentron rubrum	B	697,728	6177	163,520	1422	861,248	4	81	19
Sargocentron violaceum	A	518,827	3875	77,802	950	596,629	7	87	13

DC, double cone; SC, single cone; PR, photoreceptors. Peak values are expressed in densities mm^{-2}.

Journal of Experimental Biology (2021) 224, jeb233098. doi:10.1242/jeb.233098

Colour vision under bright- and dim-light conditions

Colour vision relies on the opponent processing of light caught by a minimum of two differently tuned photoreceptors (Kelber et al., 2003). Since rods and cones usually function at different light levels and most vertebrates possess a single rod type, colour vision is often thought to be exclusively cone based and limited to bright-light conditions. However, dim-light colour vision based on modified cones or on a combination of cones and rods does exist and has been demonstrated in geckos (Roth and Kelber, 2004) and amphibians (Yovanovich et al., 2017), respectively. Moreover, several deep-sea fishes that possess multiple rod types (de Busserolles et al., 2017; Musilova et al., 2019) and/or a multibank retina (Denton and Locket, 1989) are likely candidates for purely rod-based colour discrimination. In the case of holocentrids, nocturnal colour vision may be achieved by their multibank retina, even with a single rod type, on the assumption that each bank acts as a spectral filter (Denton and Locket, 1989). Under this scenario, each bank is assumed to have a different spectral sensitivity and colour vision is made possible by comparing the outputs of the different banks (Denton and Locket, 1989). While this is possible in theory, only behavioural experiments combined with neurophysiological measurements will be able to attest whether holocentrids use their multibank retinas for dim-light colour discrimination.

In addition to their multibank retina, Holocentridae do possess several cone types and as such also have the potential for 'classic' colour vision during the daytime. Results from this study indicate that Holocentridae possess at least two spectrally distinct cone types and therefore are likely dichromats. All species investigated here possess single cones that express the *SWS2A* gene sensitive to the blue range of the spectrum, and double cones that express one or two *RH2* genes, sensitive to the green range of the spectrum. While cone spectral sensitivity estimations made in this study were comparable to MSP measurements performed by Losey et al. (2003), some differences were observed, notably in *M. berndti* in which two different spectral sensitivities were found in double cones while only a single *RH2B* gene was expressed in the retinas of the fish from our study. The discrepancy between opsin gene expression and MSP data may be due to the different origin of the individuals studied; opsin gene expression was measured in fishes from the Great Barrier Reef while MSP was performed in fishes from Hawaii (Losey et al., 2003). Moreover, opsin gene expression, and by extension spectral sensitivities, provide a snapshot of the visual system of the animal at the time of sampling, a state that may change in teleost fishes over the course of the day (Johnson et al., 2013), between seasons (Shimmura et al., 2017) and at different habitat depths (Stieb et al., 2016). Therefore, it is possible that *M. berndti* individuals collected in February in Australia possess a different set of visual pigments to individuals collected in Hawaii in May–June. Notably, holocentrids do possess up to eight *RH2* copies in their genomes (Musilova et al., 2019), but only a maximum of three were expressed at the same time in our dataset. Additional copies could therefore be used under different light settings or at different ontogenetic stages. Further *in situ* and experimental studies combining RNA-seq and MSP will be needed to further explore this. Finally, it is important to keep in mind that although a number of mutagenesis studies have demonstrated the effects of specific tuning sites in fishes (reviewed in Takahashi and Ebrey, 2003; Yokoyama, 2008; Yokoyama and Jia, 2020), the combined effects and/or interactions of multiple tuning sites with one another remain mostly unclear and may also explain the small differences in spectral sensitivities observed between measured and predicted data.

Unlike in other coral reef fish families that show high interspecific variability in cone opsin expression (Phillips et al., 2015; Stieb et al., 2016; Luehrmann et al., 2020), variability was very low in holocentrids from the same subfamily and did not seem to correlate with habitat partitioning. Between the subfamilies, Holocentrinae had a higher proportion of cone opsin expression compared with Myripristinae and expressed two *RH2A* paralogs compared with the single *RH2B* copy expressed in Myripristinae. Since the two *RH2A* genes in Holocentrinae were found to be co-expressed in both members of the double cones and are also predicted to have similar spectral sensitivities, the advantage of expressing two copies over a single *RH2* gene is intriguing. Certainly, the higher level of cone opsin expression in Holocentrinae does suggest that they rely on their photopic visual system more than the Myripristinae. However, whether holocentrids can discriminate colour during the day remains to be investigated. The large size of their cone photoreceptors compared with diurnal species (Munz and McFarland, 1973) may also increase sensitivity to lower light conditions and allow for cone or a mixture of cone and rod-based colour vision in dim-light conditions (Hess et al., 1998). Consequently, their large cone photoreceptors and multibank retinas may enable holocentrids to perceive colour in a wide range of light intensities.

Holocentrid visual ecology

Ganglion cell topography and acuity

Retinal ganglion cell topography is a powerful tool in visual ecology, highlighting areas of high cell density and therefore high acuity in a specific part of the visual field. In teleost fishes, several studies have shown a strong link between the retinal topography pattern and the habitat and/or behavioural ecology of an animal (Collin and Pettigrew, 1988a,b, 1989; Shand et al., 2000; Collin, 2008; de Busserolles et al., 2014b). In holocentrids, ganglion cell topography showed very little intraspecific and interspecific variability within subfamilies. However, density and topography patterns differed between the two subfamilies. While both subfamilies share similar habitats (Gladfelter and Johnson, 1983), they differ in feeding ecologies, with Holocentrinae mainly feeding on benthic crustaceans and species from the genus *Myripristis* (Myripristinae) feeding on large zooplankton in the water column (Gladfelter and Johnson, 1983; Greenfield, 2002). Accordingly, an area temporalis that extends into a weak horizontal streak may allow Holocentrinae to scan and detect crustaceans situated in front of them, on or close to the sea floor. In Myripristinae, a large area temporo-ventralis that provides higher acuity in front and above of them, may instead facilitate the detection of zooplankton when seen against the background illumination. A similar ganglion cell topography and relationship with feeding mode was also observed in the nocturnal apogonids (Luehrmann et al., 2020).

In addition to the topography pattern, spatial resolving power (SRP) also differed between the two subfamilies with Holocentrinae having higher acuities than Myripristinae. However, this result has to be interpreted carefully since *Myripristis* spp. had a large population of displaced ganglion cells that was not included in the analysis, potentially resulting in an underestimation of their SRP. Displaced ganglion cells have been described in many vertebrates and shown in several cases to be part of the accessory optic system (Simpson, 1984). As such, all or some of these displaced ganglion cells are likely to have a different function to the ones found in the ganglion cell layer and may not contribute to visual acuity. Future labelling and tract tracing experiments will be needed to elucidate the function of the displaced ganglion cell population in

Myripristinae. Moreover, while displaced ganglion cells were not obvious in Holocentrinae, their presence/absence was not studied here and will need to be assessed further. Regardless, holocentrid visual acuity was relatively low compared with that of diurnal reef fishes with similar eye sizes (e.g. the SRP of *M. murdjan* and *S. rubrum* is 4.38 and 7.35 cpd, respectively, versus an SRP in *Lethrinus chrysostamus* of 22 cpd; Collin and Pettigrew, 1989). However, Holocentrids did have a similar SRP to the nocturnal apogonids (~7 cpd; Luehrmann et al., 2020). Since apogonids are much smaller fish with much smaller eyes, this suggests a higher eye investment in visual acuity for apogonids compared to holocentrids. Conversely, the large eyes in holocentrids (Schmitz and Wainwright, 2011) coupled with a short focal length (McFarland, 1991), is likely an adaptation to increase the overall sensitivity of the eye rather than its acuity.

Photoreceptor topography

Photoreceptor cells constitute the first level of visual processing and as such their density and distribution provide important information about the visual demands of a species. Even though the holocentrid retina is rod-dominated, only the density and distribution of cone photoreceptors could be assessed in this study owing to the presence of the multibank retina.

In diurnal teleost fishes that have a cone-dominated retina, cones are generally arranged in a regular pattern or mosaic. Conversely, nocturnal and bottom-dwelling fishes that have a rod-dominated retina tend to have disintegrated cone mosaics (Engström, 1963). Accordingly, holocentrids, and especially Myripristinae, were found to have a mostly disintegrated cone mosaic that fits with their nocturnal activity pattern. Holocentrinae, however, did have a more organised cone arrangement, especially in the temporal part, the area with the highest visual acuity. This, in addition to their higher cone densities, cone opsin expression and visual acuity suggest that the Holocentrinae visual system is better adapted for photopic conditions than the visual system of the Myripristinae.

Similarly to the ganglion cells, photoreceptor topography may be used to identify areas of the visual field that are ecologically meaningful for a species. While photoreceptor and ganglion cell topography usually match and have peak cell densities in the same region of the retina, variations do exist, and may indicate different visual demands in different parts of the visual field of the animal or at different times of the day (Stieb et al., 2019; Tettamanti et al., 2019). In Holocentrids, total cone and ganglion cell topographies differed, especially in Myripristinae. Since holocentrids are nocturnal fish and have a rod-dominated retina, it is likely that the topography and peak density of their rod photoreceptors matches that of their ganglion cells, as seen in some deep-sea fishes (de Busserolles and Marshall, 2017). This is supported by the highest number of banks being located in the area of the highest ganglion cell density in all three species. Unfortunately, limited information is available about holocentrid daytime activities. During that time, they appear to hover in or above their refuges and may partake in some social interactions such as courtship, aggression and predator avoidance (Winn et al., 1964; Carlson and Bass, 2000). Accordingly, a horizontal streak may allow them to scan a wide area of their visual field to look for possible intruders or conspecifics while staying within the safety of their refuges, as suggested for the highly territorial anemonefishes (Stieb et al., 2019). Moreover, a high density of cells in the nasal area, as seen in Holocentrinae, may also help in detecting predators coming from behind (Collin and Pettigrew, 1988a).

For all holocentrids, but especially in the Myripristinae, single and double cone topography differed, suggesting that the different types of cones may be used in different visual tasks. While it has been demonstrated that both single and double cones are used for colour discrimination in the coral reef Picasso triggerfish, *Rhinecanthus aculeatus* (Pignatelli et al., 2010), in many other species this is not clear (Marshall et al., 2019). Since the spectral sensitivity of double cones often matches the spectral distribution of the ambient/background light they may be used in luminance detection tasks (McFarland, 1991; Marshall et al., 2019; Carleton et al., 2020). In holocentrids, this idea is further supported by the ratio of double to single cones which was consistently higher in the dorsal retina. If double cones are indeed used in achromatic tasks, having a higher proportion in the dorsal retina, the area that samples light in the field of view below the fish where background illumination is lower, might assist in increasing sensitivity. However, behavioural tests will be needed to confirm this.

Conclusion

Holocentridae have a visual system that is well-adapted for their nocturnal lifestyle with large eyes, short focal length, rod-dominated retina, multibank retina, extremely high rod opsin expression, rods tuned to their preferred light conditions, few cone opsins that are expressed at low levels, few cone photoreceptors and relatively low visual acuity. Moreover, the fact that the holocentrid ganglion cell topography correlates with their feeding mode, a task which in this family is exclusively conducted at night, further supports their heavy reliance on their scotopic visual system. The presence of at least two spectrally different cone types with their own topography patterns also indicates the use of their cone-based visual system during the day and the potential for dichromacy. Moreover, while interspecific variability was very low within the family, differences in visual adaptations could be seen between the two subfamilies at all levels with Holocentrinae having a slightly more developed photopic visual system compared with Myripristinae. Finally, what really sets the holocentrid family apart from other coral reef fishes is their well-developed multibank retina, an adaptation mostly found in deep-sea fishes, and their potential for colour vision in a wide range of light settings, especially under scotopic conditions. Future ontogenetic and behavioural analyses should therefore be conducted in order to understand the origin and function of the multibank retina, as well as to assess whether this family is able to discriminate colours and under which light intensities. Additionally, investigation of other teleosts with intermediate depth ranges, such as mesophotic species, are likely to reveal interesting adaptations for dim-light vision.

Acknowledgements

We would like to acknowledge the Traditional Owners of Lizard Island, The Dingaal Aboriginal people. We thank Cairns Marine for supplying fish and the staff at the Lizard Island Research Station, Lorenz Sueess and Eva McClure for support during field work. We also thank Janette Edson from the Queensland Brain Institute (QBI) Genomics Facility for library preparation and transcriptome sequencing, Rumelo Amor from the QBI Advanced Microscopy Facility for technical support, Zuzana Musilová from Charles University (Czech Republic) for help with FISH experiments, Helen Cooper and Michael Langford (QBI) for providing lab facilities to conduct FISH experiments and the two anonymous reviewers and editor. The stereology were performed at the QBI Advanced Microscopy Facility using Stereo Investigator, which was supported by an ARC LIEF grant (LE100100074).

Competing interests

The authors declare no competing or financial interests.

Author contributions

Conceptualization: F.d.B., F.C., S.M.S., N.J.M.; Methodology: F.d.B., F.C., S.M.S., M.L.; Validation: F.d.B., F.C., S.M.S.; Formal analysis: F.d.B., F.C., S.M.S., L.F.,

M.L.; Investigation: F.d.B., F.C., L.F., S.M.S.; M.L., Resources: F.d.B., F.C., S.M.S., N.J.M.; Writing - original draft: F.d.B.; Writing - review & editing: F.d.B., F.C., L.F., S.M.S., M.L., N.J.M.; Visualization: F.d.B., F.C., L.F., S.M.S.; Supervision: F.d.B., N.J.M.; Project administration: F.d.B.; Funding acquisition: F.d.B., N.J.M.

Funding

This research was supported by several Australian Research Council (ARC) grants, an ARC Laureate Fellowship (FL140100197) awarded to N.J.M. and ARC DECRA awarded to F.d.B. (DE180100949) and F.C. (DE200100620). In addition, F.C. was also supported by a University of Queensland Development Fellowship and a Swiss National Science Foundation Early Postdoc Mobility Fellowship and S.M.S. was supported by the German Research Foundation (DFG).

Data availability

Raw-read transcriptomes (PRJNA674704, SAMN16670685–SAMN16670689) and single gene sequences (MW219662-MW219691) are available through GenBank (https://www.ncbi.nlm.nih.gov/genbank/). Gene alignments, phylogenies, transcriptome assemblies, sensitivity prediction alignments and additional tables and figures are available from the Dryad digital repository (de Busserolles et al., 2021): nvx0k6dr3.

Supplementary information

Supplementary information available online at
https://jeb.biologists.org/lookup/doi/10.1242/jeb.233098.supplemental

References

Afgan, E., Sloggett, C., Goonasekera, N., Makunin, I., Benson, D., Crowe, M., Gladman, S., Kowsar, Y., Pheasant, M., Horst, R. et al. (2015). Genomics Virtual Laboratory: a practical bioinformatics workbench for the Cloud. *PLoS ONE* **10**, e0140829. doi:10.1371/journal.pone.0140829

Ali, M. A. Anctil, M. (1976). *Retinas of Fishes: An Atlas*. Springer-Verlag Berlin Heidelberg.

Allison, W. T., Barthel, L. K., Skebo, K. M., Takechi, M., Kawamura, S. and Raymond, P. A. (2010). Ontogeny of cone photoreceptor mosaics in zebrafish. *J. Comp. Neurol.* **518**, 4182-4195. doi:10.1002/cne.22447

Baddeley, A. and Turner, R. (2005). Spatstat: an R package for analyzing spatial point patterns. *J. Stat. Softw.* **12**, 1-42. doi:10.18637/jss.v012.i06

Barthel, L. K. and Raymond, P. A. (2000). In situ hybridization studies of retinal neurons. In *Methods in Enzymology*, pp. 579-590. Academic Press.

Bolger, A. M., Lohse, M. and Usadel, B. (2014). Trimmomatic: a flexible trimmer for Illumina sequence data. *Bioinformatics* **30**, 2114-2120. doi:10.1093/bioinformatics/btu170

Bozzano, A. (2003). Vision in the rufus snake eel, *Ophichthus rufus*: adaptive mechanisms for a burrowing life-style. *Mar. Biol.* **143**, 167-174. doi:10.1007/s00227-003-1032-9

Carleton, K. L. and Yourick, M. R. (2020). Axes of visual adaptation in the ecologically diverse family Cichlidae. *Semin. Cell Dev. Biol.* **106**, 43-52. doi:10.1016/j.semcdb.2020.04.015

Carleton, K. L., Escobar-Camacho, D., Stieb, S. M., Cortesi, F. and Marshall, N. J. (2020). Seeing the rainbow: mechanisms underlying spectral sensitivity in teleost fishes. *J. Exp. Biol.* **223**, jeb193334. doi:10.1242/jeb.193334

Carlson, B. A. and Bass, A. H. (2000). Sonic/vocal motor pathways in squirrelfish (Teleostei, Holocentridae). *Brain Behav. Evol.* **56**, 14-28. doi:10.1159/000006674

Chan, T., Lee, M. and Sakmar, T. P. (1992). Introduction of hydroxyl-bearing amino acids causes bathochromic spectral shifts in rhodopsin. Amino acid substitutions responsible for red-green color pigment spectral tuning. *J. Biol. Chem.* **267**, 9478-9480.

Coimbra, J. P., Marceliano, M. L. V., Andrade-da-Costa, B. L. S. and Yamada, E. S. (2006). The retina of tyrant flycatchers: topographic organization of neuronal density and size in the ganglion cell layer of the Great Kiskadee *Pitangus sulphuratus* and the Rusty Margined Flycatcher *Myiozetetes cayanensis* (Aves: Tyrannidae). *Brain Behav. Evol.* **68**, 15-25. doi:10.1159/000092310

Coimbra, J. P., Trévia, N., Marceliano, M. L. V., Andrade-Da-Costa, B. L. S., Picanço-Diniz, C. W. and Yamada, E. S. (2009). Number and distribution of neurons in the retinal ganglion cell layer in relation to foraging behaviors of tyrant flycatchers. *J. Comp. Neurol.* **514**, 66-73. doi:10.1002/cne.21992

Coimbra, J. P., Nolan, P. M., Collin, S. P. and Hart, N. S. (2012). Retinal ganglion cell topography and spatial resolving power in penguins. *Brain Behav. Evol.* **80**, 254-268. doi:10.1159/000341901

Collin, S. P. (2008). A web-based archive for topographic maps of retinal cell distribution in vertebrates. *Clin. Exp. Optom.* **91**, 85-95. doi:10.1111/j.1444-0938.2007.00228.x

Collin, S. P. and Collin, H. B. (1988). Topographic analysis of the retinal ganglion cell layer and optic nerve in the sandlance *Limnichthyes fasciatus* (Creeiidae, Perciformes). *J. Comp. Neurol.* **278**, 226-241. doi:10.1002/cne.902780206

Collin, S. P. and Pettigrew, J. D. (1988a). Retinal topography in reef teleosts. I. Some species with well-developed areae but poorly-developed streaks. *Brain Behav. Evol.* **31**, 269-282. doi:10.1159/000116594

Collin, S. P. and Pettigrew, J. D. (1988b). Retinal topography in reef teleosts. II. Some species with prominent horizontal streaks and high-density areae. *Brain Behav. Evol.* **31**, 283-295. doi:10.1159/000116595

Collin, S. P. and Pettigrew, J. D. (1989). Quantitative comparison of the limits on visual spatial resolution set by the ganglion cell layer in twelve species of reef teleosts. *Brain Behav. Evol.* **34**, 184-192. doi:10.1159/000116504

Collin, S. P. and Shand, J. (2003). Retinal sampling and the visual field in fishes. In *Sensory Processing in Aquatic Environments* (ed. S. P. Collin and N. J. Marshall), pp 139-169. Springer New York.

Cortesi, F., Musilová, Z., Stieb, S. M., Hart, N. S., Siebeck, U. E., Malmstrøm, M., Tørresen, O. K., Jentoft, S., Cheney, K. L., Marshall, N. J. et al. (2015). Ancestral duplications and highly dynamic opsin gene evolution in percomorph fishes. *Proc. Natl. Acad. Sci. USA* **112**, 1493-1498. doi:10.1073/pnas.1417803112

Cortesi, F., Musilová, Z., Stieb, S. M., Hart, N. S., Siebeck, U. E., Cheney, K. L., Salzburger, W. and Marshall, N. J. (2016). From crypsis to mimicry: changes in colour and the configuration of the visual system during ontogenetic habitat transitions in a coral reef fish. *J. Exp. Biol.* **219**, 2545-2558. doi:10.1242/jeb.139501

Cronin, T. W., Johnsen, S., Marshall, N. J. and Warrant, E. J. (2014). *Visual Ecology*. Princeton University Press.

Dalton, B. E., Loew, E. R., Cronin, T. W. and Carleton, K. L. (2014). Spectral tuning by opsin coexpression in retinal regions that view different parts of the visual field. *Proceedings of the Royal Society B-Biological Sciences* **281**, 20141980. doi:10.1098/rspb.2014.1980

Dalton, B. E., Lu, J., Leips, J., Cronin, T. W. and Carleton, K. L. (2015). Variable light environments induce plastic spectral tuning by regional opsin coexpression in the African cichlid fish, *Metriaclima zebra*. *Mol. Ecol.* **24**, 4193-4204. doi:10.1111/mec.13312

Dalton, B. E., de Busserolles, F., Marshall, N. J. and Carleton, K. L. (2017). Retinal specialization through spatially varying cell densities and opsin coexpression in cichlid fish. *J. Exp. Biol.* **220**, 266-277. doi:10.1242/jeb.149211

de Busserolles, F. and Marshall, N. J. (2017). Seeing in the deep-sea: visual adaptations in lanternfishes. *Philos. Trans. R. Soc. B Biol. Sci.* **372**, 20160070. doi:10.1098/rstb.2016.0070

de Busserolles, F., Fitzpatrick, J. L., Marshall, N. J. and Collin, S. P. (2014a). The influence of photoreceptor size and distribution on optical sensitivity in the eyes of lanternfishes (Myctophidae). *PLoS ONE* **9**, e99957. doi:10.1371/journal.pone.0099957

de Busserolles, F., Marshall, N. J. and Collin, S. P. (2014b). Retinal ganglion cell distribution and spatial resolving power in deep-sea lanternfishes (Myctophidae). *Brain Behav. Evol.* **84**, 262-276. doi:10.1159/000365960

de Busserolles, F., Cortesi, F., Helvik, J. V., Davies, W. I. L., Templin, R. M., Sullivan, R. K. P., Michell, C. T., Mountford, J. K., Collin, S. P., Irigoien, X. et al. (2017). Pushing the limits of photoreception in twilight conditions: The rod-like cone retina of the deep-sea pearlsides. *Sci. Adv.* **3**, eaao4709. doi:10.1126/sciadv.aao4709

de Busserolles, F., Cortesi, F., Fogg, L., Stieb, S. M., Luehrmann, M. and Marshall, N. J. (2021). Data from The visual ecology of Holocentridae, a nocturnal coral reef fish family with a deep-sea-like multibank retina. *Dryad Dataset* doi:10.5061/dryad.nvx0k6dr3

Demski, L. S. (2003). In a fish's mind's eye: the visual pallium of teleosts. In *Sensory Processing in Aquatic Environments* (ed. S. P. Collin and N. J. Marshall), pp. 404-419. New York, NY: Springer New York.

Denton, E. J. and Locket, N. A. (1989). Possible wavelength discrimination by multibank retinae in deep-sea fishes. *J. Mar. Biol. Assoc. U.K.* **69**, 409-435. doi:10.1017/S0025315400029507

Douglas, R. H. and Djamgoz, M. B. A. (1990). *The Visual System of Fish*. Chapman and Hall.

Engström, K. (1963). Cone types and cone arrangements in teleost retinae. *Acta Zool.* **44**, 179-243. doi:10.1111/j.1463-6395.1963.tb00408.x

Fasick, J. I. and Robinson, P. R. (1998). Mechanism of spectral tuning in the dolphin visual pigments. *Biochemistry* **37**, 433-438. doi:10.1021/bi972500j

Fishelson, L., Ayalon, G., Zverdling, A. and Holzman, R. (2004). Comparative morphology of the eye (with particular attention to the retina) in various species of cardinal fish (Apogonidae, Teleostei). *Anat. Rec. A Discov. Mol. Cell. Evol. Biol.* **277A**, 249-261. doi:10.1002/ar.a.20005

Fricke, R., Eschmeyer, W. N. and Fong, J. D. (2020). Eschmeyer's Catalog of Fishes: species by family/subfamily. Electronic version accessed dd mmm 2020. (http://researcharchive.calacademy.org/research/ichthyology/catalog/SpeciesByFamily.asp).

Fröhlich, E. and Wagner, H. J. (1998). Development of multibank rod retinae in deep-sea fishes. *Vis. Neurosci.* **15**, 477-483. doi:10.1017/S095252389815304X

Garza Gisholt, E., Hemmi, J. M., Hart, N. S. and Collin, S. P. (2014). A comparison of spatial analysis methods for the construction of topographic maps of retinal cell density. *PLoS ONE* **9**, e93485. doi:10.1371/journal.pone.0093485

Gladfelter, W. B. and Johnson, W. S. (1983). Feeding niche separation in a guild of tropical reef fishes (Holocentridae). *Ecology* **64**, 552-563. doi:10.2307/1939975
Glaser, E. M. and Wilson, P. D. (1998). The coefficient of error of optical fractionator population size estimates: a computer simulation comparing three estimators. *J. Microsc.* **192**, 163-171. doi:10.1046/j.1365-2818.1998.00417.x
Gordon, J., Shapley, R. M. and Kaplan, E. (1978). The eel retina. Receptor classes and spectral mechanisms. *J. Gen. Physiol.* **71**, 123-138. doi:10.1085/jgp.71.2.123
Greenfield, D. W. (2002). Holocentridae: squirrelfishes (soldierfishes). In *The living marine resources of the Western Central Atlantic*, Vol. 5 (ed. K. E. Carpenter), pp. 1192-1202. Rome: FAO Species Identification Guide for Fishery Purposes and American Society of Ichthyologists and Herpetologists Special Publication.
Greenfield, D. W., Randall, J. E. and N, P. P. (2017). A review of the soldierfish genus *Ostichthys* (Beryciformes: Holocentridae), with descriptions of two new species from Myanmar. *J. Ocean Sci. Found.* **26**, 1-33.
Haas, B. J., Papanicolaou, A., Yassour, M., Grabherr, M., Blood, P. D., Bowden, J., Couger, M. B., Eccles, D., Li, B., Lieber, M. et al. (2013). De novo transcript sequence reconstruction from RNA-seq using the Trinity platform for reference generation and analysis. *Nat. Protocols* **8**, 1494-1512. doi:10.1038/nprot.2013.084
Hess, M., Melzer, R. R. and Smola, U. (1998). The photoreceptors of *Muraena helena* and *Ariosoma balearicum* - A comparison of multiple bank retinae in anguilliform eels (Teleostei). *Zool. Anz.* **237**, 127-137.
Hughes, A. (1975). A quantitative analysis of the cat retinal ganglion cell topography. *J. Comp. Neurol.* **163**, 107-128. doi:10.1002/cne.901630107
Hunt, D., Hankins, M. W., Collin, S. P. and Marshall, N. J. (2014). *Evolution of Visual and Non-Visual Pigments*. Springer.
Janz, J. M. and Farrens, D. L. (2001). Engineering a functional blue-wavelength-shifted rhodopsin mutant. *Biochemistry* **40**, 7219-7227. doi:10.1021/bi002937i
Johnson, A. M., Stanis, S. and Fuller, R. C. (2013). Diurnal lighting patterns and habitat alter opsin expression and colour preferences in a killifish. *Proc. R. Soc. B* **280**, 20130796. doi:10.1098/rspb.2013.0796
Katoh, K. and Standley, D. M. (2013). MAFFT multiple sequence alignment software version 7: improvements in performance and usability. *Mol. Biol. Evol.* **30**, 772-780. doi:10.1093/molbev/mst010
Katoh, K., Misawa, K., Kuma, K. i. and Miyata, T. (2002). MAFFT: a novel method for rapid multiple sequence alignment based on fast Fourier transform. *Nucleic Acids Res.* **30**, 3059-3066. doi:10.1093/nar/gkf436
Kelber, A., Vorobyev, M. and Osorio, D. (2003). Animal colour vision – behavioural tests and physiological concepts. *Biol. Rev.* **78**, 81-118. doi:10.1017/S1464793102005985
Lamb, T. D. (2013). Evolution of phototransduction, vertebrate photoreceptors and retina. *Prog. Retin. Eye Res.* **36**, 52-119. doi:10.1016/j.preteyeres.2013.06.001
Landgren, E., Fritsches, K., Brill, R. and Warrant, E. (2014). The visual ecology of a deep-sea fish, the escolar *Lepidocybium flavobrunneum* (Smith, 1843). *Phil. Trans. R. Soc. B Biol. Sci.* **369**, 20130039. doi:10.1098/rstb.2013.0039
Lin, S. W., Kochendoerfer, G. G., Carroll, K. S., Wang, D., Mathies, R. A. and Sakmar, T. P. (1998). Mechanisms of spectral tuning in blue cone visual pigments: visible and raman spectroscopy of blue-shifted rhodopsin mutants. *J. Biol. Chem.* **273**, 24583-24591. doi:10.1074/jbc.273.38.24583
Locket, N. A. (1985). The multiple bank rod fovea of *Bajacalifornia drakei*, an alepocephalid deep-sea teleost. *Proc. R. Soc. Lond. B Biol. Sci.* **224**, 7-22. doi:10.1098/rspb.1985.0018
Losey, G. S., McFarland, W. N., Loew, E. R., Zamzow, J. P., Nelson, P. A. and Marshall, N. J. (2003). Visual biology of Hawaiian coral reef fishes. I. Ocular transmission and visual pigments. *Copeia* **2003**, 433-454. doi:10.1643/01-053
Luehrmann, M., Carleton, K. L., Cortesi, F., Cheney, K. L. and Marshall, N. J. (2019). Cardinalfishes (Apogonidae) show visual system adaptations typical of nocturnally and diurnally active fish. *Mol. Ecol.* **28**, 3025-3041. doi:10.1111/mec.15102
Luehrmann, M., Cortesi, F., Cheney, K. L., de Busserolles, F. and Marshall, N. J. (2020). Microhabitat partitioning correlates with opsin gene expression in coral reef cardinalfishes (Apogonidae). *Funct. Ecol.* **00**, 1-12. doi:10.1111/1365-2435.13529
Lythgoe, J. N. (1979). *The Ecology of Vision*. Oxford: Clarendon Press.
Marshall, N. J. and Vorobyev, M. (2003). The design of color signals and color vision in fishes. In *Sensory Processing in Aquatic Environments* (ed. S. P. Collin and N. J. Marshall), pp. 194-222. New-York: Springer-Verlag.
Marshall, N. J., Cortesi, F., de Busserolles, F., Siebeck, U. E. and Cheney, K. L. (2019). Colours and colour vision in reef fishes: Past, present and future research directions. *J. Fish Biol.* 95, 5-38. doi:10.1111/jfb.13849
Matsumoto, Y., Fukamachi, S., Mitani, H. and Kawamura, S. (2006). Functional characterization of visual opsin repertoire in Medaka (*Oryzias latipes*). *Gene* **371**, 268-278. doi:10.1016/j.gene.2005.12.005
Matthiessen, L. (1882). Über die Beziehungen, welche zwischen dem Brechungsindex des Kernzentrums der Krystalllinse und den Dimensionen des Auges bestehen. *Pflügers Archiv für die gesamate Physiologie des Menschen und der Tiere* **27**, 510-523. doi:10.1007/BF01802978
McFarland, W. N. (1991). The visual world of coral reef fishes. In *The Ecology of Fishes on Coral Reefs* (ed. P. F. Sale), pp. 16-38. Academic Press.
Meyer-Rochow, V. B. and Coddington, P. A. (2003). Eyes and vision of the New Zealand torrentfish *Cheimarrichthys fosteri* VON HAAST (1874): histology, photochemistry and electrophysiology. In *Fish Adaptations* (ed. A. L. Val and B. G. Kapoor), pp. 337-383. Oxford and IBH Publ. & M/s Sci. Publ.
Miller, M. A., Pfeiffer, W. and Schwartz, T. (2010). Creating the CIPRES Science Gateway for inference of large phylogenetic trees. *2010 Gateway Computing Environments Workshop (GCE)*, New Orleans, LA, pp 1-8.
Munz, F. W. and McFarland, W. N. (1973). The significance of spectral position in the rhodopsins of tropical marine fishes. *Vision Res.* **13**, 1829-1874. doi:10.1016/0042-6989(73)90060-6
Musilova, Z., Cortesi, F., Matschiner, M., Davies, W. I. L., Patel, J. S., Stieb, S. M., de Busserolles, F., Malmstrøm, M., Tørresen, O. K., Brown, C. J. et al. (2019). Vision using multiple distinct rod opsins in deep-sea fishes. *Science* **364**, 588-592. doi:10.1126/science.aav4632
Nicol, J. A. C., Arnott, H. J. and Best, A. C. G. (1973). Tapeta lucida in bony fishes (Actinopterygii): a survey. *Can. J. Zool.* **51**, 69-81. doi:10.1139/z73-012
Omura, Y. and Yoshimura, R. (1999). Immunocytochemical Localization of Taurine in the Developing Retina of the Lofteye Flounder *Paralichthys olivaceus*. *Arch. Histol. Cytol.* **62**, 441-446. doi:10.1679/aohc.62.441
Omura, Y., Tsuzuki, K., Sugiura, M., Uematsu, K. and Tsukamoto, K. (2003). Rod cells proliferate in the eel retina throughout life. *Fisheries Science* **69**, 924-928. doi:10.1046/j.1444-2906.2003.00708.x
Palczewski, K., Kumasaka, T., Hori, T., Behnke, C. A., Motoshima, H., Fox, B. A., Trong, I. L., Teller, D. C., Okada, T., Stenkamp, R. E. et al. (2000). Crystal structure of rhodopsin: a G protein-coupled receptor. *Science* **289**, 739-745. doi:10.1126/science.289.5480.739
Pankhurst, N. (1989). The relationship of ocular morphology to feeding modes and activity periods in shallow marine teleosts from New Zealand. *Environ. Biol. Fishes* **26**, 201-211. doi:10.1007/BF00004816
Parry, J. W. L., Carleton, K. L., Spady, T., Carboo, A., Hunt, D. M. and Bowmaker, J. K. (2005). Mix and match color vision: tuning spectral sensitivity by differential opsin gene expression in Lake Malawi cichlids. *Curr. Biol.* **15**, 1734-1739. doi:10.1016/j.cub.2005.08.010
Phillips, G. A. C., Carleton, K. L. and Marshall, N. J. (2015). Multiple genetic mechanisms contribute to visual sensitivity variation in the Labridae. *Mol. Biol. Evol.* **33**, 201-215. doi:10.1093/molbev/msv213
Pignatelli, V., Champ, C., Marshall, J. and Vorobyev, M. (2010). Double cones are used for colour discrimination in the reef fish, *Rhinecanthus aculeatus*. *Biol. Lett.* **6**, 537-539. doi:10.1098/rsbl.2009.1010
Raymond, P. A. and Barthel, L. K. (2004). A moving wave patterns the cone photoreceptor mosaic array in the zebrafish retina. *Int. J. Dev. Biol.* **48**, 935-945. doi:10.1387/ijdb.041873pr
Ronquist, F., Teslenko, M., van der Mark, P., Ayres, D. L., Darling, A., Höhna, S., Larget, B., Liu, L., Suchard, M. A. and Huelsenbeck, J. P. (2012). MrBayes 3.2: efficient Bayesian phylogenetic inference and model choice across a large model space. *Syst. Biol.* **61**, 539-542. doi:10.1093/sysbio/sys029
Roth, L. S. V. and Kelber, A. (2004). Nocturnal colour vision in geckos. *Proc. R. Soc. B* **271**, S485-S487. doi:10.1098/rsbl.2004.0227
Schmitz, L. and Wainwright, P. C. (2011). Nocturnality constrains morphological and functional diversity in the eyes of reef fishes. *BMC Evol. Biol.* **11**, 338. doi:10.1186/1471-2148-11-338
Shand, J. (1994a). Changes in retinal structure during development and settlement of the goatfish *Upeneus tragula*. Brain. *Behav. Evol.* **43**, 51-60. doi:10.1159/000113624
Shand, J. (1994b). *Changes in the Visual System of Teleost Fishes During Growth and Settlement: An Ecological Perspective*. James Cook University.
Shand, J. (1997). Ontogenetic changes in retinal structure and visual acuity: a comparative study of coral-reef teleosts with differing post-settlement lifestyles. *Environ. Biol. Fishes* **49**, 307-322. doi:10.1023/A:1007353003066
Shand, J., Chin, S. M., Harman, A. M., Moore, S. and Collin, S. P. (2000). Variability in the location of the retinal ganglion cell area centralis is correlated with ontogenetic changes in feeding behavior in the black bream, *Acanthopagrus butcheri* (Sparidae, Teleostei). *Brain Behav. Evol.* **55**, 176-190. doi:10.1159/000006651
Shapley, R., Gordon, J. and Denton, E. J. (1980). The visual sensitivity of the retina of the conger eel. *Proc. R. Soc. Lond. B Biol. Sci.* **209**, 317-330. doi:10.1098/rspb.1980.0097
Shimmura, T., Nakayama, T., Shinomiya, A., Fukamachi, S., Yasugi, M., Watanabe, E., Shimo, T., Senga, T., Nishimura, T., Tanaka, M. et al. (2017). Dynamic plasticity in phototransduction regulates seasonal changes in color perception. *Nat. Commun.* **8**, 7. doi:10.1038/s41467-017-00432-8
Siebeck, U. E., Collin, S. P., Ghoddusi, M. and Marshall, N. J. (2003). Occlusable corneas in toadfishes: light transmission, movement and ultrastruture of pigment during light- and dark-adaptation. *J. Exp. Biol.* **206**, 2177-2190. doi:10.1242/jeb.00401
Simpson, J. I. (1984). The accessory optic system. *Annu. Rev. Neurosci.* **7**, 13-41. doi:10.1146/annurev.ne.07.030184.000305
Stieb, S. M., Carleton, K. L., Cortesi, F., Marshall, N. J. and Salzburger, W. (2016). Depth dependent plasticity in opsin gene expression varies between damselfish (Pomacentridae) species. *Mol. Ecol.* **25**, 3645-3661. doi:10.1111/mec.13712
Stieb, S. M., Cortesi, F., Sueess, L., Carleton, K. L., Salzburger, W. and Marshall, N. J. (2017). Why UV vision and red vision are important for damselfish

(Pomacentridae): structural and expression variation in opsin genes. *Mol. Ecol.* **26**, 1323-1342. doi:10.1111/mec.13968

Stieb, S. M., de Busserolles, F., Carleton, K. L., Cortesi, F., Chung, W. S., Dalton, B. E., Hammond, L. A. and Marshall, N. J. (2019). A detailed investigation of the visual system and visual ecology of the Barrier Reef anemonefish, Amphiprion akindynos. *Sci. Rep.* **9**, 14. doi:10.1038/s41598-019-52297-0

Stone, J. (1981). *The Whole Mount Handbook: a Guide to the Preparation and Analysis of Retinal Whole Mounts*. Sydney: Maitland Publications.

Takahashi, Y. and Ebrey, T. G. (2003). Molecular basis of spectral tuning in the newt short wavelength sensitive visual pigment. *Biochemistry* **42**, 6025-6034. doi:10.1021/bi020629

Taylor, S. M. and Grace, M. S. (2005). Development of retinal architecture in the elopomorph species *Megalops atlanticus*, *Elops saurus* and *Albula vulpes* (Elopomorpha: Teleostei). *Contrib. Mar. Sci.* **37**, 1-29.

Taylor, S. M., Loew, E. R. and Grace, M. S. (2015). Ontogenic retinal changes in three ecologically distinct elopomorph fishes (Elopomorpha:Teleostei) correlate with light environment and behavior. *Vis. Neurosci.* **32**, E005. doi:10.1017/S0952523815000024

Tettamanti, V., de Busserolles, F., Lecchini, D., Marshall, N. J. and Cortesi, F. (2019). Visual system development of the spotted unicornfish, *Naso brevirostris* (Acanthuridae). *J. Exp. Biol.* **222**, jeb209916. doi:10.1242/jeb.209916

Thorpe, A., Douglas, R. H. and Truscott, R. J. W. (1993). Spectral transmission and short-wave absorbing pigments in the fish lens - I. Phylogenetic distribution and identity. *Vision Res.* **33**, 289-300. doi:10.1016/0042-6989(93)90085-B

Toller, W. W. (1996). *Rhodopsin Evolution in the Holocentridae (Pisces: Beryciformes)*. University of Southern California.

Toyama, M., Hironaka, M., Yamahama, Y., Horiguchi, H., Tsukada, O., Uto, N., Ueno, Y., Tokunaga, F., Seno, K. and Hariyama, T. (2008). Presence of rhodopsin and porphyropsin in the eyes of 164 fishes, representing marine, diadromous, coastal and freshwater species—a qualitative and comparative study†. *Photochem. Photobiol.* **84**, 996-1002. doi:10.1111/j.1751-1097.2008.00344.x

Ullmann, J. F. P., Moore, B. A., Temple, S. E., Fernandez-Juricic, E. and Collin, S. P. (2011). The retinal wholemount technique: a window to understanding the brain and behaviour. *Brain Behav. Evol.* **79**, 26-44. doi:10.1159/000332802

Wagner, H.-J., Fröhlich, E., Negishi, K. and Collin, S. P. (1998). The eyes of deep-sea fish II. Functional morphology of the retina. *Prog. Retin. Eye Res.* **17**, 637-685. doi:10.1016/S1350-9462(98)00003-2

Walls, G. L. (1942). *The Vertebrate Eye and its Adaptive Radiation*. Bloomfield Hills: The Cranbrook Institute of Science.

Warrant, E. J. and Locket, N. A. (2004). Vision in the deep sea. *Biol. Rev.* **79**, 671-712. doi:10.1017/S1464793103006420

Warrant, E. J., Collin, S. P. and Locket, N. A. 2003. Eye disign and vision in deep-sea fishes. In *Sensory Processing in Aquatic Environments* (ed. S. P. Collin and N. J. Marshall), pp. 303-322. New York: Springer-Verlag.

West, M. J., Slomianka, L. and Gundersen, H. J. G. (1991). Unbiased stereological estimation of the total number of neurons in the subdivisions of the rat hippocampus using the optical fractionator. *Anat. Rec.* **231**, 482-497. doi:10.1002/ar.1092310411

Winn, H. E., Marshall, J. A. and Hazlett, B. (1964). Behavior, diel activities, and stimuli that elicit sound production and reactions to sounds in the longspine squirrelfish. *Copeia* **1964**, 413-425. doi:10.2307/1441036

Yokoyama, S. (2008). Evolution of dim-light and color vision pigments. *Annu. Rev. Genomics Hum. Genet.* **9**, 259-282. doi:10.1146/annurev.genom.9.081307.164228

Yokoyama, S. and Jia, H. (2020). Origin and adaptation of green-sensitive (RH2) pigments in vertebrates. *FEBS Open Bio* **10**, 873-882. doi:10.1002/2211-5463.12843

Yokoyama, S. and Tada, T. (2003). The spectral tuning in the short wavelength-sensitive type 2 pigments. *Gene* **306**, 91-98. doi:10.1016/S0378-1119(03)00424-4

Yokoyama, S. and Takenaka, N. (2004). The molecular basis of adaptive evolution of squirrelfish rhodopsins. *Mol. Biol. Evol.* **21**, 2071-2078. doi:10.1093/molbev/msh217

Yokoyama, S., Tada, T., Zhang, H. and Britt, L. (2008). Elucidation of phenotypic adaptations: Molecular analyses of dim-light vision proteins in vertebrates. *Proc. Natl Acad. Sci. USA* **105**, 13480-13485. doi:10.1073/pnas.0802426105

Yovanovich, C. A. M., Koskela, S. M., Nevala, N., Kondrashev, S. L., Kelber, A. and Donner, K. (2017). The dual rod system of amphibians supports colour discrimination at the absolute visual threshold. *Phil. Trans. R. Soc. B Biol. Sci.* **372**, 20160066. doi:10.1098/rstb.2016.0066

Supplementary Information

Table S1. Primers used for probe template (length of at least 600 bases) design. RNA Polymerase promoter sequences (T7 resp. T3) were incorporated in primer sequences.

Species	Opsin	Primer	Sequence
N. sammara	*SWS2*	SWS2_forward	5'-TAATACGACTCACTATAGGGATCACTCAGCCCGTTCTTGG-3'
		SWS2_reverse	5'-AATTAACCCTCACTAAAGGGCTCAGATCGAAGGTCTGCCC-3'
	RH2A-1	RH2A-1_forward	5'- TAATACGACTCACTATAGGGAAACCTTCGATGTGGACTGAAT-3'
		RH2A-1_reverse	5'-AATTAACCCTCACTAAAGGGGACACCTGTCAGGGCATTCC-3'
	RH2A-2	RH2A-2_forward	5'-TAATACGACTCACTATAGGGTAACCCTCGATGTGGACTGAGC -3'
		RH2A-2_reverse	5'-AATTAACCCTCACTAAAGGGTTCATCATGGCAAACTCCAACA-3'
M. berndti	*SWS2A*	SWS2A_forward	5'-TAATACGACTCACTATAGGGCTCAGGACCACTTGGGGAAC-3'
		SWS2A_reverse	5'-AATTAACCCTCACTAAAGGGGACTGGCTGATGACTCCTCG-3'
	RH2B	RH2B_forward	5'-TAATACGACTCACTATAGGGTGGTGGTCACAGCTCAGAAC-3'
		RH2B_reverse	5'-AATTAACCCTCACTAAAGGGACCATGCCACCCATTCCAAT-3'

Table S2. Summary of the stereology parameters used for the ganglion cell and photoreceptor topography analyses. SL = standard length, ∅ = diameter, DC = double cone, SC = single cone, CE = Schaeffer coefficient of error.

Ganglion cells

Species	Indiv	SL (cm)	Lens ∅ (mm)	Counting frame (µm x µm)	Grid (µm x µm)	CE
M. berndti	A	15.3	8.5	200 x 200	1700 x 1700	0.034
	B	16.5	9.4	200 x 200	1800 x 1800	0.037
M. violacea	A	12	6.5	150 x 150	1300 x 1300	0.032
	B	9.3	5.3	150 x 150	1050 x 1050	0.027
M. murdjan	A	15.7	8.8	200 x 200	1700 x 1700	0.035
M. pralinia	A	12.2	8.3	200 x 200	1600 x 1600	0.029
N. sammara	A	11.9	5.5	130 x 130	1150 x 1150	0.053
	B	14.3	6.7	130 x 130	1300 x 1300	0.056
S. spiniferum	A	19.7	7.1	150 x 150	1350 x 1350	0.045
	B	21.8	7.2	150 x 150	1400 x 1400	0.043
S. diadema	A	11.9	5.1	120 x 120	940 x 940	0.044
	B	11.7	5.0	120 x 120	1000 x 1000	0.048
S. rubrum	A	15.7	8.0	150 x 150	1450 x 1450	0.045
S. violaceum	A	15.6	6.6	150 x 150	1250 x 1250	0.041

Photoreceptors

Species	Indiv	SL (cm)	Counting frame DC (µm x µm)	Counting frame SC (µm x µm)	Grid (µm x µm)	CE DC	CE SC
M. berndti	C	10.2	150 x 150	300 x 300	1160 x 1160	0.030	0.037
M. violacea	B	9.3	150 x 150	300 x 300	1350 x 1350	0.028	0.050
	C	10.7	150 x 150	300 x 300	1250 x 1250	0.033	0.050
M. murdjan	B	14.7	300 x 300	450 x 450	1400 x 1400	0.035	0.057
	C	18.1	300 x 300	300 x 300	1750 x 1750	0.030	0.053
M. pralinia	A	12.2	300 x 300	300 x 300	1500 x 1500	0.035	0.063
N. sammara	A	11.9	130 x 130	260 x 260	1050 x 1050	0.027	0.033
	C	10.4	130 x 130	260 x 260	1000 x 1000	0.030	0.033
S. spiniferum	A	19.7	150 x 150	300 x 300	1370 x 1370	0.028	0.034
S. diadema	C	10.8	150 x 150	300 x 300	1080 x 1080	0.027	0.042
	D	11.7	150 x 150	300 x 300	950 x 950	0.039	0.049
S. rubrum	B	14	150 x 150	300 x 300	1200 x 1200	0.030	0.039
S. violaceum	A	15.6	200 x 200	400 x 400	1260 x 1260	0.025	0.038

Table S3. Summary of holocentrid transcriptomes, opsin gene mapping, and proportional opsin gene expression. *RH1* = rod opsin, *SWS2* = short-wavelength sensitive, *RH2* = rhodopsin-like. * Transcriptomes from Musilova et al. 2019.

	RNA sequencing Transcriptome			Mapping # filtered reads					Proportional opsin gene expression %					
				Rod	Single cones	Double cones (sub-mapping)			Rod vs Cone		Cone opsin vs total cone expression			
Holocentrinae	**ID**	**SRA Acc. No.**	**# raw (filter) reads**	***RH1***	***SWS2A***	***RH2A-1***	***-2***	***-3***	**R**	**C**	***SWS2A***	***RH2A-1***	***-2***	***-3***
Sargocentron spiniferum Lizard Island	F2	SAMN16670685	19,118,407 (14,126,874)	2,260,377	1,748	14,764 (1,064)	17611 (1,712)	496 (32)	98.5	1.5	5.1	36	57.9	1.1
Sargocentron rubrum Cairns Marine	F37	SAMN16670686	34,314,266 (23,032,335)	2,179,239	4,996	41,880 (3,190)	46779 (4,742)	-	95.9	4.1	5.4	38.1	56.6	-
Sargoceontron diadema Cairns Marine	F30	SAMN16670687	18,791,321 (13,400,810)	1,073,406	4,354	41,214 (1,528)	5866 (1970)	-	91.7	8.3	4.5	41.2	54.3	-
*Neoniphon sammara** Lizard Island	F3	SRX5060694	6,838,760 (6,264,679)	324,704	834	8,250 (90)	7,434 (70)	-	95.2	4.8	5.1	53.4	41.5	-
	F6	SRX5060695	4,506,938 (4,001,509)	170,140	422	4,240 (40)	3,942 (52)	-	95.2	4.8	4.9	41.3	53.7	-
	F10	SRX5060692	4,084,557 (3,464,740)	176,987	760	6,825 (116)	5,866 (66)	-	93.0	7.0	5.7	60.1	34.2	-
								Mean	**94.9**	**5.1**	**5.1**	**45.0**	**49.7**	**-**
								s.e.m.	**1.0**		**0.2**	**3.9**	**3.9**	**-**
Myripristinae				***RH1***	***SWS2A***	***RH2B-1***			**R**	**C**	***SWS2A***	***RH2B-1***		
*Myripristis jacobus** Cape Verde	51	SRS4076665	17,244,006 (10,058,945)	912,891	386	7,363			99.1	0.9	4.9	95.1		
	53	SRS4076643	32,578,163 (25,511,374)	1,926,830	732	4,910			99.7	0.3	12.8	87.2		
*Myripristis berndti** Lizard Island	F7	SRS4076646	8,753,048 (6,071,712)	377,066	54	876			99.8	0.3	5.7	94.3		
	F8	SRS4076637	6,812,942 (5,841,804)	541,184	98	1,682			99.7	0.3	5.4	94.6		
	F11	SRS4076678	5,848,153 (5,271,695)	336,736	162	1,816			99.4	0.6	8.1	91.9		
	F12	SRS4076668	4,810,822 (4,282,905)	362,974	126	1,972			99.4	0.6	5.9	94.1		
Myripristis murdjan Lizard Island	F31	SAMN16670688	26042977 (19969212)	2,497,905	1,076	19,185			99.2	0.8	5.2	94.8		
Myripristis violacea Lizard Island	F5	SAMN16670689	18679367 (13576628)	1,835,739	825	11,467			99.3	0.7	6.6	93.4		
								Mean	**99.4**	**0.6**	**6.8**	**93.2**		
								s.e.m.	**0.1**		**0.9**			

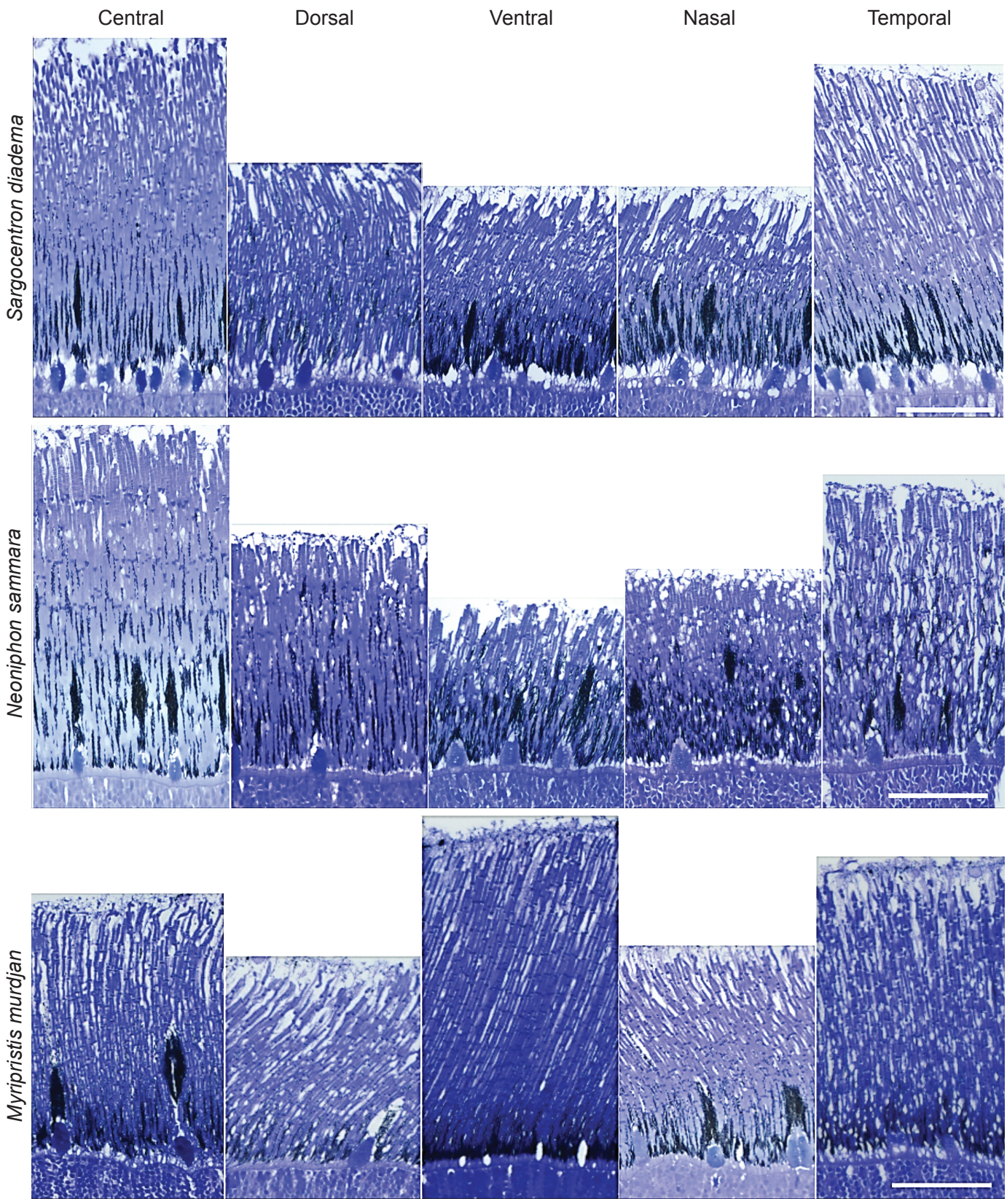

Figure S1. Variation in the number of banks and thickness of the photoreceptor layer across the retina of three species of Holocentridae. Scale bar = 50 μm.

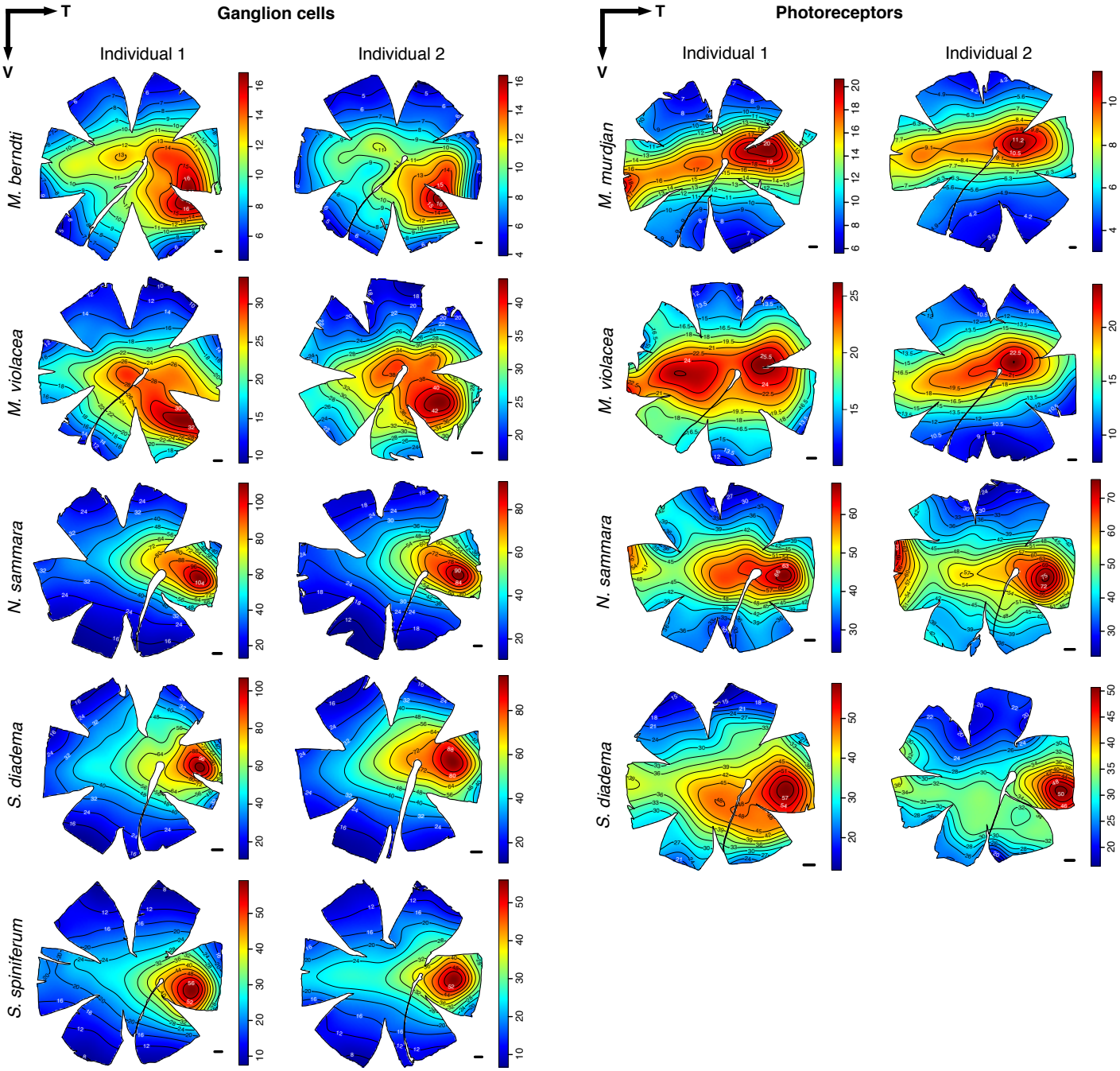

Figure S2. Intraspecific variability in the topographic distribution of ganglion cell and photoreceptor densities in the retinas of several species of Holocentridae. The black lines represent iso-density contours and values are expressed in densities x 10^2 cells/mm2. The black arrow indicates the orientation of the retinas. T = temporal, V = ventral. Scale bars = 1 mm.

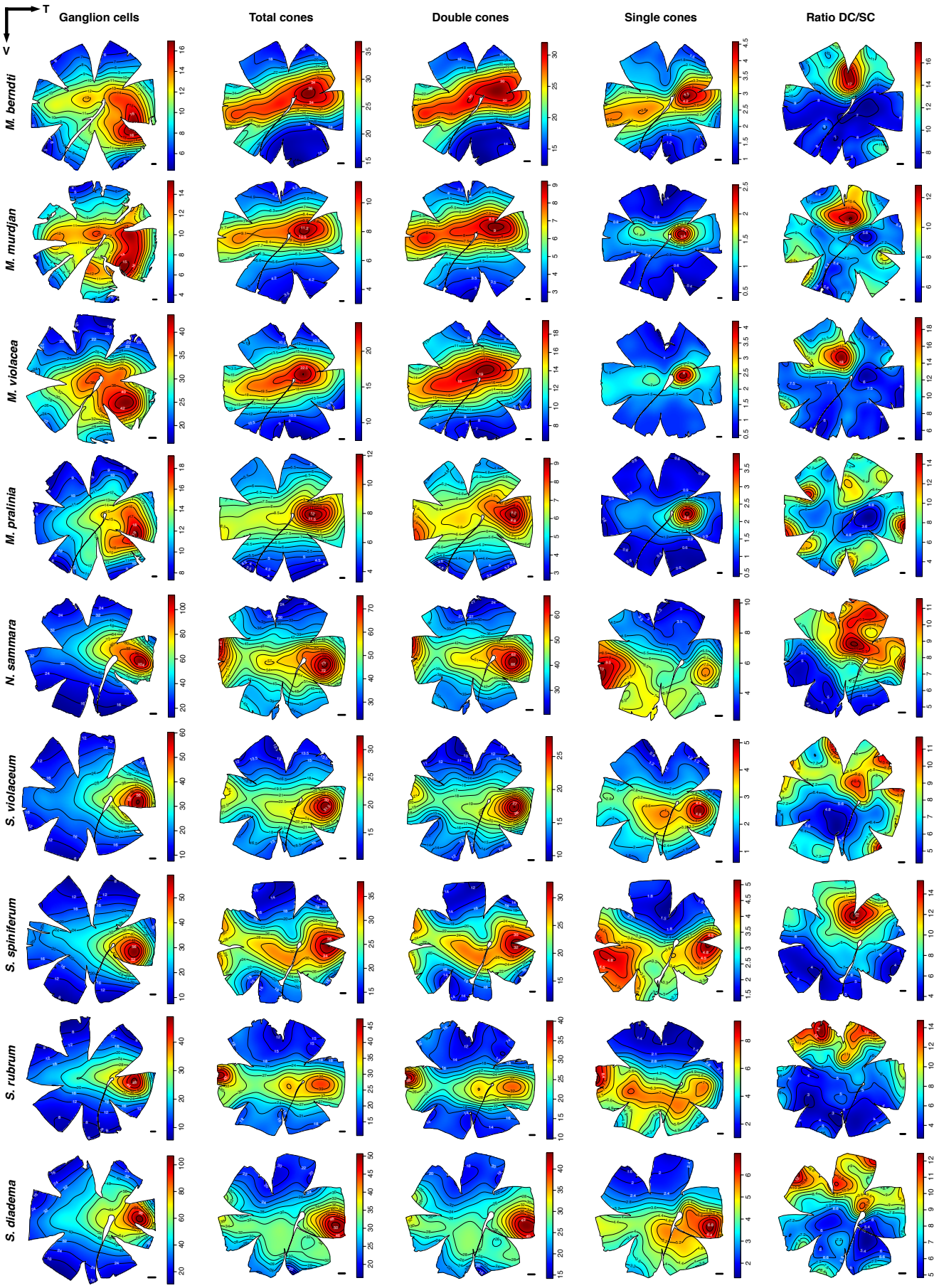

Figure S3. Topographic distribution of ganglion cell densities in the retinas of nine species of Holocentridae: The black lines represent iso-density contours and values are expressed in densities x 10^2 cells/mm^2, except for ratio DC/SC. The black arrow indicates the orientation of the retinas. T = temporal, V = ventral. Scale bars = 1 mm.